

BL1A

Local Environment Analysis of Al Atoms in Proton-Conducting Amorphous Aluminum Phosphate Thin Films

Y. Aoki and H. Habazaki

Graduate School of Engineering, Hokkaido University, N13W8, Sapporo 060-8628, Japan

Inorganic phosphate compounds are attractive as an unhydrated proton conductor due to the presence of large number of native acid sites. Thin film of such materials has potential as an electrolyte membrane of next-generation intermediate temperature fuel cell. The conventional proton-conducting inorganic phosphate compounds are basically polycrystalline, and they have serious problem in forming the gas-tight membrane due to the difficulty in sintering. recently, we discovered that amorphous aluminum phosphate thin films exhibit the enhanced proton conductivity in nonhumidified atmosphere in the intermediate temperature range [1]. Amorphous metal oxides have intrinsic advantages for their application to thin film electrolyte, since they tend to be non-granular, dense layer without void formation at grain boundary due to the covalently-bonded M-O-M-O network. The study on the local environment of metal atoms are critical for identifying the protonic active sites in this film. Here, we study the local environment of Al atoms in amorphous zirconium phosphate thin films by Al K-edge XAS in order to identify the protonic active site.

Amorphous aluminum phosphate thin film, $a\text{-AlP}_m\text{O}_x$, was prepared on an ITO substrate (Aldrich) by multiple spin-coating of precursor solutions of phosphorous oxide (P_2O_5) (Kanto) and aluminum *sec*-butoxide ($\text{Al}(\text{O}^i\text{Bu})_3$) (Kanto) at the Al/Si atomic ratio of 3/2, 1/1, 1/2 and 1/3. The metal concentration (Al+P) in the precursor mixture sol was adjusted in 50 mM. A film with thickness of 100 nm was prepared from both of these sols. The precursor sols were spin-coated onto the ITO substrate at 3000 rpm for 40 sec by a Mikasa 1H-D7 spin coater. The deposited gel layer was hydrolyzed by blowing hot air for 30 sec (Iuchi hot gun), and the substrate was cooled to room temperature by blowing cold air for 20 sec. These cycles of spin-coating, hydrolysis and cooling were repeated 10-20 times and the gel film thus obtained was calcined at 400°C for 15 min. The combination of deposition and calcination was repeated more than 3 times, and the final calcination was performed at 450°C for 1 h.

Al K-edge XAS spectroscopy was carried out with $a\text{-AlP}_m\text{O}_x$ films of 100 nm-thickness (Figure 1). It is reported that Al K-edge spectra is very sensitive to the coordination number and geometry of AlO_x moieties in oxides.[1] Here, the Y-zeolite (Wako) was used as a reference material of tetrahedral AlO_4 configuration and $\alpha\text{-Al}_2\text{O}_3$ (Wako) as that of octahedral AlO_6 configuration, respectively. Y-zeolite shows a sharp

peaks at 1566 eV due to the transition from 1s to 3d unoccupied states and a broad peak at 1571 eV attributed to the six-coordinated Al atoms given by water adsorption [2]. These features are in agreement with the spectral features of tetrahedral AlO_4 compounds. $\alpha\text{-Al}_2\text{O}_3$ shows two sharp peaks at 1568 and 1572 eV, which are identical to the features of the compound given by the previous reports. The Al K-edge spectra of $a\text{-AlP}_m\text{O}_x$ films ($m = 0.67, 1.0, 2.0$ and 3.0) were drastically changed by Al/P atomic ratio. In $m = 0.67$ and 1.0, the film show a sharp peak at around 1566.5 eV, indicating that Al atoms inside film preferably take the tetrahedral AlO_4 configuration. However, the film with $m = 1.0$ and 2.0 apparently show an additional peak at higher-energy side of the main peak. This feature indicates that a part of Al atoms form octahedral AlO_6 configuration in these films. These results suggest that coordination environment of Al atoms in aluminophosphate films is changed from tetrahedral to octahedral with increasing phosphorous content m . The detail structure of phosphate groups will be investigated by P L-edge XAS.

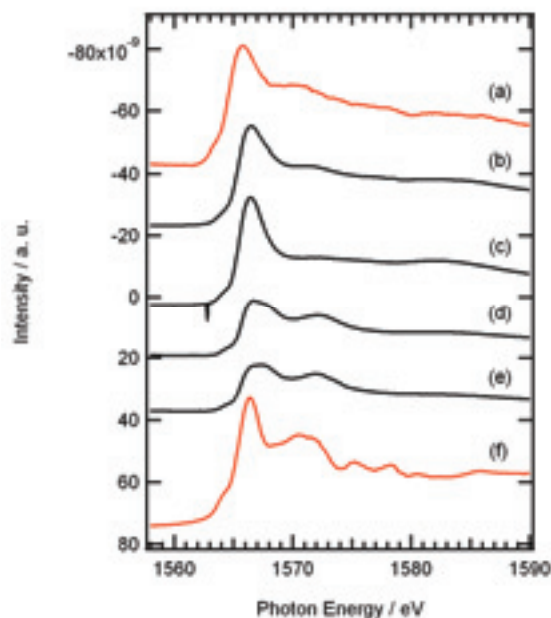


Fig. 1. Al K-edge XAS spectra of amorphous AlP_mO_x films of 100 nm-thickness and reference materials. (a) Y-zeolite powder, (b) $\text{AlP}_{0.67}\text{O}_x$, (c) AlPO_x , (d) AlP_2O_x , (e) AlP_3O_x and (f) $\alpha\text{-Al}_2\text{O}_3$ powder.

[1] Y. Kato *et al.*, PCCP **3** (2001) 1925.

[2] A. Omegna *et al.*, J. Phys. Chem. B **109** (2005) 9280.

Asymmetric Synthesis and Decomposition of Amino Acids by Using UVSOR-FEL

K. Kobayashi¹, S. Shima¹, T. Suzuki¹, T. Kaneko¹, H. Mita², J. Takahashi³, M. Hosaka⁴, M. Adachi⁵, H. Zen⁵ and M. Katoh⁵

¹Graduate School and Faculty of Engineering, Yokohama National University, Yokohama 240-8501, Japan

²Faculty of Engineering, Fukuoka Institute of Technology, Fukuoka 811-0295, Japan

³NTT Microsystem Integration Laboratories, Atsugi 243-0198, Japan

⁴Graduate School of Engineering, Nagoya University, Nagoya 464-8601, Japan

⁵Institute for Molecular Science, Okazaki 444-8585, Japan

Introduction

Terrestrial organisms basically use L-Amino acids and D-sugars. The origin of homochirality of biomolecules remains one of the largest riddles in the study of the origin of life. A number of hypotheses have been presented on the origin of biochemical homochirality. Finding of the enantiomeric excesses (*e. e.*'s) of certain amino acids in carbonaceous chondrites suggested that there were some physical sources to induce them in space. Recently Fukue *et al.* reported extended high circular polarization in the Orion massive star forming region [1]. It is of interest to examine possible generation of *e. e.*'s of amino acids by circularly polarized light. In order to examine this hypothesis, we irradiated amino acids or metal complexes of amino acids with circularly polarized ultraviolet light (CPL-UV) from a free-electron laser (FEL) of UVSOR. We chose two amino acids as targets: Isovaline (IVal), a non-proteinous amino acid which has α -methyl group in place of α -hydrogen atom, was selected since relatively large *e. e.* of IVal was found in Murchison meteorite [2]. A small *e. e.* formed by CPL-UV might have been enlarged by autocatalytic reactions in primordial ocean. From such a point of view, histidine (His), was used because it has catalytic activity. Aqueous solution of His, IVal, and metal complexes of them were irradiated with CPL-UV. Thin films of DL-His were also irradiated with CPL-UV.

Experimental

Aqueous solution of IVal, His, or copper complex of His (*pH* = 3, 7 or 11 in all cases) was irradiated with CPL-UV at 215 nm from an FEL of UVSOR II (IMS, Japan). DL-Amino acids were determined by HPLC.

Vacuum-evaporated thin films of DL-His were also irradiated with CPL-UV (Fig. 1). After the irradiation, optical anisotropy of the resulting thin films were observed with circular dichroism (CD) spectra.

Results and Discussion

After the irradiation with the CPL on DL-His film, no clear peaks appeared in the CD spectra from 170 to 300 nm region. This result suggests that photolysis of His film by the CPL-UV is more difficult than the cases of alanine (Ala) and IVal. In previous report, we reported that DL-Ala film after CPL-UV irradiation exhibited CD peaks with an opposite sign at 180 and 215 nm [3]. Theoretical investigation using *ab initio* quantum-chemistry calculations for alanine suggests that the emergence of CD peaks by CPL irradiation is derived from asymmetric dimerization of alanine molecular.

E. e.'s were not observed after CPL-UV irradiation to acidic / neutral amino acid solutions, but some *e. e.*'s were observed in the case of basic solutions. It was suggested that *pH* of the irradiated solution is an important parameter of chirogenesis by CPL-UV. In order to confirm the present results, further studies including more precise separation methods for DL-amino acids were required.



Fig. 1. Irradiation of amino acid film with CPL-UV from FEL.

[1] T. Fukue, *et al.*, *Origins Life Evol. Biosph.*, in press (2010).

[2] J. R. Cronin and S. Pizzarello, *Science* **275** (1997) 951.

[3] J. Takahashi *et al.*, *Int. J. Mol. Sci.* **10** (2009) 3044.

Local Environment Analysis of P Atoms in Proton-Conducting Amorphous Zirconium Phosphate Thin Films

Y. Aoki and H. Habazaki

Graduate School of Engineering, Hokkaido University, N13W8, Sapporo 060-8628, Japan

Inorganic phosphate compounds are attractive as an unhydrated proton conductor due to the presence of large number of native acid sites. Thin film of such materials has potential as an electrolyte membrane of next-generation intermediate temperature fuel cell. The conventional proton-conducting inorganic phosphate compounds are basically polycrystalline, and they have serious problem in forming the gas-tight membrane due to the difficulty in sintering. Previously, we reported that amorphous zirconium phosphate thin films exhibit the enhanced proton conductivity in nonhumidified atmosphere in the intermediate temperature range [1]. In addition, the films hydrated by heating in moisture at 400°C exhibit the increment of conductivity by two orders of magnitude. Amorphous metal oxides have intrinsic advantages for their application to thin film electrolyte, since they tend to be non-granular, dense layer without void formation at grain boundary due to the covalently-bonded M-O-M-O network. This superior conductivity is speculated to be related to the structure of phosphate groups. Here, we study the local environment of P atoms in amorphous zirconium phosphate thin films by P K-edge XANES in order to identify the protonic active site.

The amorphous zirconium phosphate, α -ZrP_{2.5}O_x, films were prepared on an ITO substrate (Aldrich) by multiple spin-coating of precursor solutions of tetrabutoxyzirconium (Zr(OⁿBu)₄) (Kanto) and phosphorous oxide (P₂O₅) (Kanto) at the Zr/P atomic ratio of 1/3. The details of the procedure were described elsewhere. [1] The metal concentration (Zr+P) in the precursor mixture sol was adjusted in 50 mM. The precursor sols were spin-coated onto the ITO substrate at 3000 rpm for 40 sec by a Mikasa 1H-D7 spin coater. The deposited gel layer was hydrolyzed by blowing hot air for 30 sec (luchi hot gun), and the substrate was cooled to room temperature by blowing cold air for 20 sec. These cycles of spin-coating, hydrolysis and cooling were repeated 10-20 times and the gel film thus obtained was calcined at 400°C for 30 min. The combination of deposition and calcination was repeated more than 3 times, and the final calcination was performed at 450°C for 2 h. The hydrated films were prepared by heating them at 450°C for 12 h in H₂O/air ($p_{\text{H}_2\text{O}} = 4.2$ kPa)

P K-edge XANES spectroscopy was carried out with α -ZrP_{2.5}O_x films of 40 nm, 100 nm and 300 nm-thickness (Figure 1). It is reported that P K-edge spectra of inorganic phosphate salts is very sensitive to the counter metal cation [2]. α -ZrP_{2.5}O_x films show a clear peak at 2154 eV and a lower-energy, pre-edge

peak at around 2151 eV in agreement with the spectral features of various phosphate salts [2]. These peaks correspond to the transition from P 1s P 3p-dominant unoccupied states which satisfy the dipole selection rule. The α -ZrP_{2.5}O_x films possess the same features of XANES in every thickness. Furthermore, the apparent change in spectra was not observed between the as-prepared and hydrated films. These results indicate the possibility that the polymerization degree, n , of phosphate group P_nO_{3n+1} does not change through the hydration. P L-edge XAS should be carried out in order to identify n in these thin films.

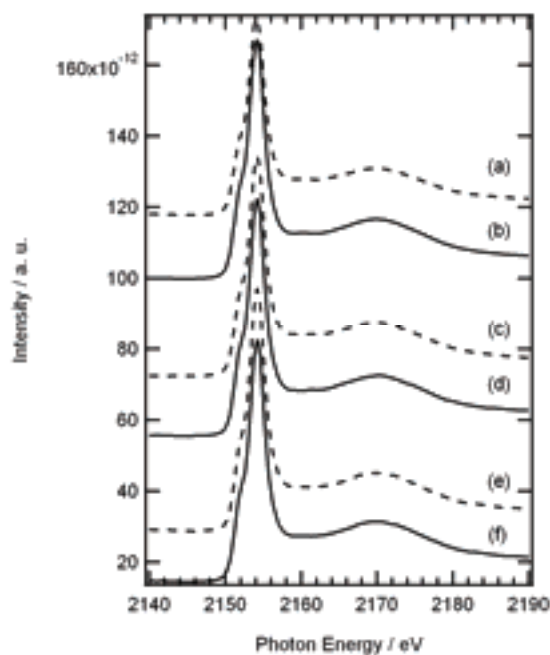


Fig. 1. P K-edge XANES spectra of amorphous ZrP_{2.5}O_x film with thickness of (a) and (b) 40 nm, (c) and (d) 100 nm and (e) and (f) 300 nm. Solid line indicates as-prepared film and dashed line hydrated film.

[1] Y. Li *et al.*, Adv. Mater. **20** (2008) 2398.

[2] N. Okude, J. Electron Spectrosc. Relat. Phenom. **101-103** (1999) 607.

Mo L_{III}-Edge XANES Study of Mo/H-MFI Catalysts for Methane Dehydroaromatization: Formation of Active Mo Carbide Species

H. Aritani¹, K. Nagashima¹, Y. Isozumi¹ and A. Nakahira²

¹Faculty of Engineering, Saitama Institute of Technology, Fukaya 369-0293, Japan

²Graduate School of Engineering, Osaka Prefecture University, Sakai 599-8531, Japan

A Mo/H-MFI catalyst shows high activity for methane dehydroaromatization in absence of oxygen. Because the catalytic system is of great value as a direct GTL (gas to liquid) process, noble catalysts with high and durable activity have been called for. Many workers have been revealed that reduction of Mo species is brought about in contact with methane in initial step. Reduced Mo ions tend to react methane to form carbide and/or oxycarbide species [1] in next step. The carbide species is active for methane dehydroaromatization, however, deactivation is brought about by carbon deposition on the catalyst surface at the same time. Ichikawa et al. [2] revealed that hydrogen co-feed gives a significant suppression effect for coking in methane conversion. On the other hand, excess hydrogen may affect a reduction of Mo species, and decrease of Mo-oxycarbide species² may give low reactivity. Thus the effect of hydrogen with methane is very important to give an effect on Mo state on H-MFI. This study addresses the effects of reaction temperature on methane dehydroaromatization over Mo/H-MFI catalysts. Mo L_{III}-edge XANES studies [3] were introduced to characterize the active Mo species on H-MFI after the methane dehydroaromatization.

Catalysts were prepared by impregnation of H-MFI support with MoO₂(acac)₂-CHCl₃ solution, and followed by drying overnight and calcination at 773 K for 3 h. Amount of MoO₃-loading is 5.0 wt% in this study. H-MFI supports with Si/Al₂ = 40–1880 were synthesized hydrothermally at 413 K for a week, and followed by ion-exchanging with NH₄Cl and calcination at 873 K. Crystallinity of Bulk phase on the whole catalysts before/after the catalytic reaction was evaluated by powdery X-ray diffraction (Rigaku, RINT2300). Amount of coking carbon was evaluated by means of thermogravimetry (Rigaku TG8120). Mo L_{III}-edge XANES spectra were measured in BL1A of UVSOR-IMS in a total-electron yield mode. Photon energy was calibrated by using Mo metal-foil at Mo L_{III}-edge, and normalized XANES spectra and their second derivatives are presented.

For Mo/H-MFI catalysts, high activity is shown in low Si/Al₂ ratio (less than 90) on H-MFI supports. In case of Mo/H-MFI in Si/Al₂=72, high and durable activity is shown at 973 K. In this case, Mo-oxycarbide species are formed during the reaction, as reported [4] previously. For the Mo/H-MFI catalysts, both high CH₄ conversion and rapid deactivation are brought about at 1023 K. At 1073 K, CH₄ conversion is scarcely seen because of sudden carbon deposition on Mo/H-MFI. Figure 1 shows the Mo L-edge XANES spectra of Mo/H-MFI

(after reaction at 973–1073 K) and reference Mo compounds. At 973 K, the Mo species consist of so-called oxycarbide species; *i.e.*, partly carbided Mo species are formed as the highly active species. At 1023 K, crystallized α -Mo₂C species are dominant. In addition, excess reduction (to form metallic/carbide species) is brought about at 1073 K. From these results, origin of the deactivation on Mo/H-MFI catalysts is not only carbon deposition but also excess reduction of Mo species to form carbide and/or metallic ones. At 973K, appropriate Mo species are formed by reduction with CH₄ to form amorphous Mo-carbide/oxycarbide species. It is concluded that the amorphous carbide/oxycarbide act as high and durable Mo species on H-MFI. Crystallization of Mo-carbide species affects the deactivation.

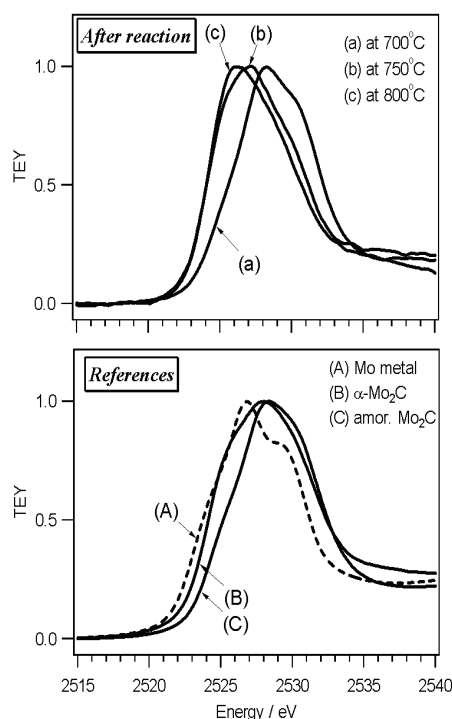


Fig. 1. Mo L_{III}-edge XANES spectra of MoO₃ (5wt%)/H-MFI(Si/Al₂=72) after CH₄ dehydroaromatization at various temperatures.

- [1] W. Li *et al.*, *J. Catal.* **191** (2000) 373.
- [2] H. Ma *et al.*, *Catal. Lett.* **89** (2003) 143.
- [3] H. Aritani *et al.*, *Chem. Lett.* **35** (2006) 416.
- [4] H. Aritani *et al.*, *UVSOR Activity Report*, **36** (2009) 113.

Study of Local Structures of Mg and Al in Hydrotalcite on Rehydration

A. Nakahira and T. Monden

Faculty of Engineering, Osaka Prefecture University, Sakai 599-8531, Japan

Layered double hydroxides (LDHs) is known as anionic clay, which is a class of lamellar compounds made up of positively charged hydroxide layers with charge balancing anions and water molecules between the layers. LDHs are expected to be useful for a large number of applications as catalyst, heavy metal ion removal, and bio-associated materials etc. Rehydration method is a one of conventional techniques of intercalation of specific anions for LDHs. It is important to clarify of local structure of LDHs on rehydration process. The investigation for the microstructures and Mg and Al local structure of LDHs in rehydration process were attempted with measurement of XANES of LDHs.

Mg/Al- CO_3 LDHs was synthesized by co-precipitation method and it was calcinated at 500°C . Rehydration process was carried out with aqueous solution of magnesium acetate. Obtained samples were identified by XRD and FT-IR. Mg K-edge XANES spectra were obtained in a total electron yield mode at room temperature using a KTP double-crystal monochromator at BL01A of the UVSOR. The spectra were collected in the photon energy range from 1300 to 1330 eV at intervals of 0.05 eV with a dwell time of 1 s.

LDH and rehydrated sample had LDH structure and calcined sample had MgO like structure by XRD and FT-IR.

Figure 1 shows the results of Mg K-edge XANES of various LDH samples: samples prepared by co-precipitation method (a), sample calcinated at 500°C (b), and samples rehydrated with aqueous solution of magnesium acetate (c). The spectrum of the samples was obviously different between each samples. From figure 1, the Mg local structures of LDH samples obtained after rehydration was similar to LDH before rehydration, suggesting that the local structure of Mg in LDHs was kept after rehydration process.

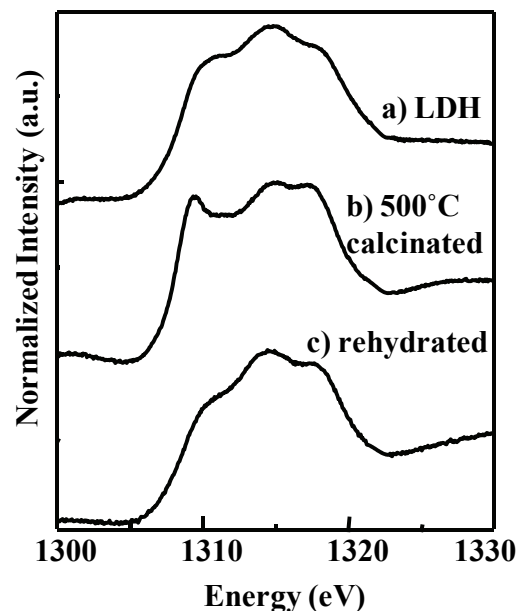


Fig. 1. Mg K-edge XANES spectra of LDHs; a) prepared by co-precipitation method, b) calcinated at 500°C , c) rehydrated with aqueous solution of magnesium acetate.

Investigation of Nanosheet in Mg/Al Type LDH Clay

A. Nakahira, T. Monden and S. Yamamoto

Faculty of Engineering, Osaka Prefecture University, Sakai 599-8531, Japan

Layered double hydroxides (LDHs) is one of important clay which is represented with the formula $[M^{2+}_{1-x}M^{3+}_x(OH)_2][A^{n-}_{x/n}mH_2O]$ (M^{2+} and M^{3+} are divalent and trivalent metals within the host layers of hydroxide sheets, and A^{n-} is an interlayer anion). Recently, the development of synthesis of hybrid LDH attracted much attention. In special, LDHs nanosheets are expected to be useful as a novel nanomaterial with various functionalities from their unique structures.

Here we synthesized LDH nanosheets by the rehydration of LDH materials heat-treated at 300 to 500 °C. In addition on the view point of the reduction of environmental load, it is important for development of a practical processing to synthesize LDHs nanosheets in aqueous system and investigate structures of LDHs nanosheets. XANES of LDHs nanosheets. was measured in order to investigate microstructures and Mg local structure.

LDH (DHT-6, Kyowa Chemical Industry Co.) was prepared as starting materials. It was calcined at 500 °C for 2 h. Calcined sample was rehydrated with aqueous solution of magnesium acetate. LDH and rehydrated LDH were calcined at 200 to 400 °C in air atmosphere for 2h. Mg K-edge XANES spectra were obtained in a total electron yield mode at room temperature using a KTP double-crystal monochromator at BL01A of the UVSOR. The spectra were collected in the photon energy range from 1300 to 1330 eV at intervals of 0.05 eV with a dwell time of 1 s.

Water dispersions of rehydrated LDH showed tyndall phenomenon and gel formation. These features indicate that LDH nanosheets were the successfully synthesized. Figure 1 shows the results of Mg K-edge XANES spectra of LDHs and rehydrated LDHs calcined at 200 to 400 °C. These XANES spectrum of the samples were obviously different between LDHs and rehydrated LDHs. Therefore, it is estimated that Mg-local structure for rehydrated LDHs having nanosheet structure are different of ones for normal LDH.

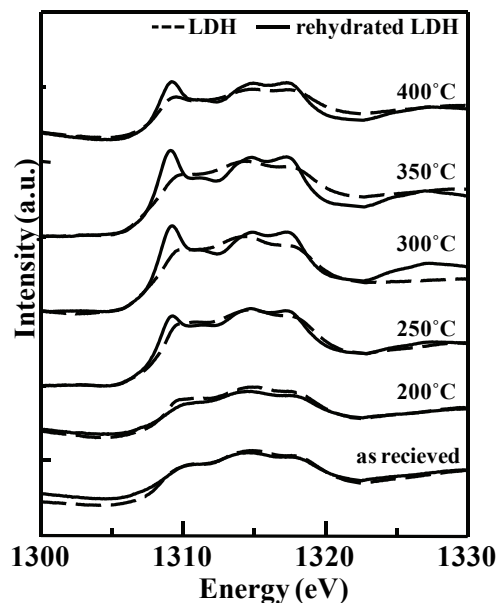


Fig. 1. Mg K-edge XANES spectra of LDH and rehydrated LDH.

Investigation of Local Structure of P K-Edge in Calcium Hydrogen Phosphate Dihydrates (DCPD) and Chitosan Composite

T. Onoki¹, S. Yamamoto¹, T. Moriguchi¹, Y. Kawabe¹, M. Sato² and A. Nakahira^{1,2}

¹Graduate School of Engineering, Osaka Prefecture University, Sakai 599-8531, Japan

²Osaka Center for Industrial Materials Research, Institute for Materials Research, Tohoku University, Sakai 599-8531, Japan

Human bone has an organic/inorganic composite structure. Bone replacing biomedical materials, for example hydroxyapatite (HA) ceramics, has been required more biocompatibility and optimal mechanical properties. Recently, bioceramics were fabricated by some hydrothermal techniques at low temperature [1, 2]. Calcium hydrogen phosphate dihydrate (DCPD) is one of starting materials for HA ceramics through a hydrothermal hot-pressing technique at around 100°C [2]. Chitosan was one of organic materials derived from crab shell. So we conducted for making an organic material composite HA ceramics for more biocompatibility and improving mechanical properties. As a first step, chitosan containing DCPD was prepared. In the present study, the structure evaluation of composite materials composed of (DCPD) and chitosan.

In this work, co-precipitation method was employed in order to prepare DCPD and chitosan composite materials. The DCPD was prepared by mixing 1.0M calcium nitrate solution (99.0%; $\text{Ca}(\text{NO}_3)_2 \cdot 4\text{H}_2\text{O}$, KANTO CHEMICAL, Japan) and 1.0M diammonium hydrogen phosphate solution (98.5%; $(\text{NH}_4)_2\text{HPO}_4$; KANTO CHEMICAL, Japan). Chitosan powder (LLWP Grade, KIMICA, Japan) was dissolved in water with a little acetic acid. The chitosan solution was added to $\text{Ca}(\text{NO}_3)_2 \cdot 4\text{H}_2\text{O}$ solution with various concentration before mixing to the $(\text{NH}_4)_2\text{HPO}_4$ solution. The mixing was carried out at a room temperature (approximately 20°C). In order to control the value of pH, acetic acid and ammonia solution were added. The precipitate from the mixture was filtered and washed with deionized water and acetone. The washed filter cake was oven-dried at 50°C for 24h, and then the dried cake was ground to a powder.

P K-edge XANES spectra for the DCPD powder were obtained in a total electron yield mode at room temperature using a InSb double-crystal monochromator at BL1A station of UVSOR. The spectra were collected in the photon energy range from 2120-2190 eV at intervals of 0.05eV with a dwell time of 1s. P-K edge XANES of the DCPD and chitosan composite powder with various concentration was shown in Figure 1. A change of the spectral patterns was not clearly observed within any preparative conditions of chitosan concentration. This result showed that the electronic structures of the phosphate ion in these composite materials are almost

same. It is needed that not only XANES but also EXAFS spectra analysis has been done.

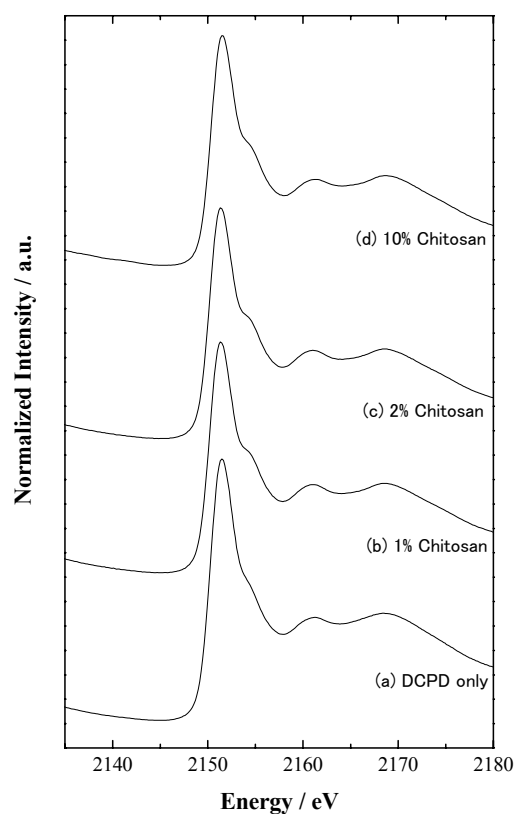


Fig. 1. XANES spectra of P K-edge of the DCPD powder with various concentration of chitosan.

[1] S. Ishihara, T. Matsumoto, T. Onoki, T. Sohmura and A. Nakahira, *Mater. Sci. Eng. C* **29** (2009) 1885-1888.

[2] T. Onoki, K. Hosoi and T. Hashida, *Scr. Mater.* **52** (2005) 767-770.

Total Photon Yield Measurement of Mg K-Edge XANES Spectrum

T. Yamamoto¹ and K. Kawabata²

¹*Faculty of Science and Engineering, Waseda University, Shinjuku 169-8555, Japan*

²*Department of Holistic Sciences, Kwansei Gakuin University, Nishinomiya 662-8501, Japan*

There are three types of popular methods to measure the X-ray absorption near-edge structure (XANES) spectrum, which are transmission, total electron yield (TEY) and total fluorescence or photon yield (TFY or TPY) methods. Among these methods, TEY is employed especially for the soft X-ray XANES, because it is difficult for such soft X-ray to pass through the sample and fluorescence yield of such energy region is quite low. However, TEY is surface sensitive detecting method like the X-ray photoelectron and Auger spectroscopy. This type of methods has disadvantages, when obtaining the electronic structure of bulk. For such purpose, TFY or TPY measurements are more suitable. Then we tried to measure Mg-K XANES of MgO before and after calcination by TEY and TPY methods to investigate the influence of surface hydration of the sample on the spectral profiles.

Mg-K XANES spectra of MgO and Mg(OH)₂ were observed at BL1A in UVSOR by TEY and TPY methods. Two types of MgO sample powders were prepared; 1) kept in air and 2) calcined just before the XANES measurements. The incident beam was monochromatized with a beryl (10 $\bar{1}$ 0) ($2d = 15.965 \text{ \AA}$) double crystal monochromator. For the TPY measurements, GaAsP photodiode (Hamamatsu Photonics) was used as a total photon yield detector.

Observed Mg-K XANES spectra of MgO before and after calcination by TEY method are shown in Fig. 1 together with that of Mg(OH)₂. From this comparison, slight difference between the spectra of MgO before and after calcination. Certain contribution of Mg(OH)₂ on peak C can be seen in the spectrum of MgO before calcination. TPY spectrum seems to contain no contribution of Mg(OH)₂ as shown in c).

We also performed the first-principles calculation for MgO by using the augmented plane wave plus local orbitals (APW+lo) package, WIEN2k [1]. Here the 3x3x3 supercell of rock-salt structured primitive cell is employed and core-hole effect is fully introduced. Calculated Mg-K XANES spectrum is also shown in Fig. 1. The calculated spectral profile has best reproduced the TPY spectrum.

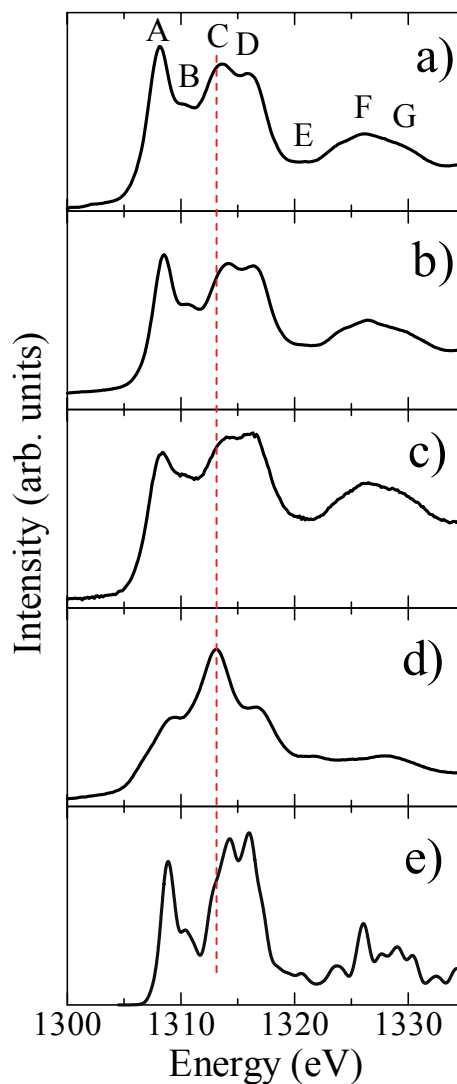


Fig. 1. Observed Mg-K XANES spectra of MgO a) before and b) after calcination by total electron yield method and by c) total photon yield method. That for d) Mg(OH)₂ and e) calculated spectrum are also shown.

[1] P. Blaha, K. Schwarz, G. Madsen, D. Kvasnicka and J. Luitz, WIEN2k, An Augmented Plane Wave + Local Orbital Program for Calculating Crystal Properties (Karlheinz Schwarz, Techn. Universitat Wien, Austria, 2001. ISBN 3-9501031-1-2)

Luminescence Properties of CsI:Ag⁻ and CsI:Au⁻ Crystals up to the Vacuum Ultraviolet Energy Region

T. Kawai¹ and T. Hirai²

¹Graduate School of Science, Osaka Prefecture University, Osaka 599-8531, Japan

²Graduate School of Science and Engineering, Ritsumeikan University, Kusatsu 525-8577, Japan

CsI:TI⁺ crystals have been well-known as the scintillator for γ -ray and their luminescence properties have been widely studied from the viewpoint of applications of this material as a phosphor. Recently, products containing toxicant heavy elements such as Tl and Pb are avoided from the viewpoint of environment. In this study, we have investigated the luminescence properties of CsI doped with Ag⁻ and Au⁻ ions without toxicity. The Au⁻ and Ag⁻ ions have the outermost s² electronic configuration in the ground state and belong to a family of TI⁺-type ions [1, 2]. Therefore, even at room temperature (RT), CsI crystals doped with the Au⁻ and Ag⁻ ions are expected to exhibit the intense luminescence from the relaxed excited-states of the sp electronic configuration.

The Ag⁻ and Au⁻ ions are not naturally present in CsI crystals. Therefore, a special treatment is needed in order to produce the negative ions. The detailed preparation of CsI:Au⁻ and CsI:Ag⁻ crystals was described elsewhere [1, 2]. The luminescence and excitation spectra up to the vacuum ultraviolet (VUV) energy region were measured at the BL-1B line of UVSOR.

Figure 1 (a) and (b) show the luminescence spectra of CsI:Ag⁻ and CsI:Au⁻ under the excitation on the energy below and above the band-gap of CsI bulk crystal. Under the excitation below the band-gap (red lines), the luminescence bands from the relaxed excited-states in impurities ions are observed at 2.46 and 2.64 eV for CsI:Ag⁻ and CsI:Au⁻, respectively. Under the excitation above the band-gap (blue lines), on the other hand, both the crystals exhibit the broader luminescence bands over the visible energy region.

In CsI:TI⁺ crystals, the broad luminescence band over the visible energy region has been attributed to the self-trapped exciton (STE) perturbed by the TI⁺ ions [3]. Since the excitation above the band-gap of CsI induces the STE, the broad luminescence spectra of CsI:Ag⁻ and CsI:Au⁻ might be attributed to the STE perturbed by the Ag⁻ and Au⁻ ions, respectively.

Figure 2 shows the excitation spectra for the visible luminescence of CsI:Au⁻ and CsI:Ag⁻ up to the VUV energy region. The remarkable response on the excitation spectra can be seen in the energy region below about 6.0 eV. The remarkable response is attributed to the intraionic transitions in the impurity ions. On the other hand, the response in the VUV energy region above the band-gap of CsI is weak.

However, the weak response in the VUV energy region indicates that photo-excited carriers and/or excitons migrate beside the impurity ions and transfer energy before self-trapping.

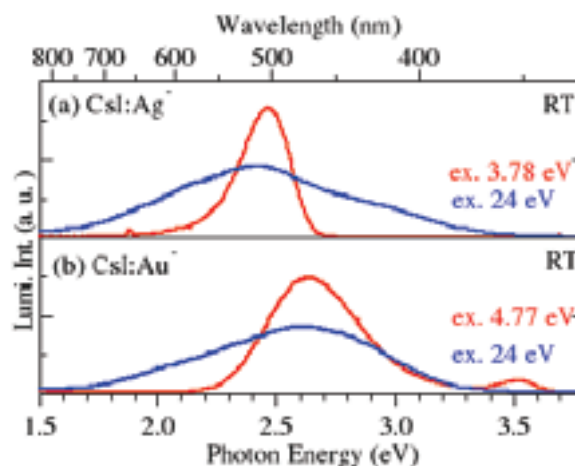


Fig. 1. Luminescence spectra of (a) CsI:Ag⁻ and (b) CsI:Au⁻ at the different excitation energies.

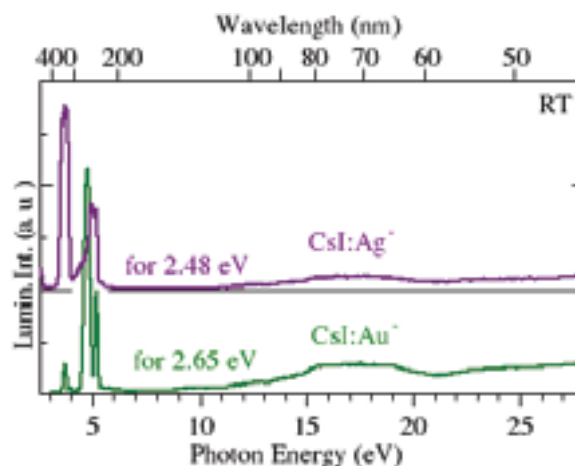


Fig. 2. Excitation spectra for the visible luminescence of CsI:Ag⁻ and CsI:Au⁻ at RT.

[1] S. Shimanuki and T. Kawai: Phys. Stat. Sol. (b) **168** (1991) 367.

[2] S. Shimanuki, M. Watanabe and T. Kawai, Phys. Stat. Sol. (b) **208** (1998) 105.

[3] V. Nagirnyi, S. Zazubovich, V. Zepelin, M. Nikl, and G. P. Pazzi, Chem. Phys. Lett. **227** (1994) 533.

Time-Resolved Luminescence of BaCl₂ under VUV Excitation

M. Koshimizu, K. Onodera and K. Asai

Department of Applied Chemistry, Graduate School of Engineering, Tohoku University, Sendai 980-8579, Japan

In recent years, the demand for fast scintillation materials has increased for applying in radiation detectors with an excellent timing property and the ability to operate at a high counting rate. BaCl₂ is a promising scintillation material having fast response. Thus far, we have revealed the scintillation properties of BaCl₂ [1]. Scintillation photons with wavelength ranging from 250-600 nm were observed with two luminescence bands at 310 and 410 nm. The scintillation time profiles consisted of two lifetime components. The shorter component had a lifetime of 1.6 ns, while the longer one had a lifetime of several tens of nanoseconds.

We have analyzed the luminescence properties of BaCl₂ under VUV excitation in order to reveal the origin of each scintillation component [2, 3]. A prominent band was observed at 410 nm under the excitation of almost the entire range of wavelengths region investigated, and it was revealed that this band is extrinsic, because this band was excited with sub-band-gap radiation. In addition, we observed a band at 310 nm under the excitation of only 170–190 nm, and this band was possibly a result of self-trapped excitons. Thus, the origins of two bands in scintillation spectrum were successfully analyzed. In this study, we analyzed the luminescence decay kinetics of BaCl₂ under VUV excitation in order to reveal the entire scintillation process in this material from the viewpoints of spectral and kinetic data.

A single crystal of BaCl₂ was grown by the Bridgman method. Luminescence time profile at each wavelength was measured with a monochromator and a photo-multiplier tube. The time profiles were measured at room temperature under the irradiation of synchrotron radiation having energies of 4–32 eV at the UVSOR facility (BL-1B) operating in single bunch mode.

Figure 1 shows the luminescence time profiles at various wavelengths under excitation at 158 nm. A weak subnanosecond decay component was observed at the entire wavelength region, and is possibly attributed to intraband luminescence. Unfortunately, we cannot observe the decay kinetics corresponding to the longer scintillation lifetime component, because the lifetime is expected to be comparable to the repetition interval of the excitation pulse of 176 ns.

Figure 2 shows the luminescence time profiles at 310 nm under VUV excitation at various wavelengths. In addition to the subnanosecond component, another component with a lifetime of 1.4 ns was observed only at the excitation wavelength of 170 – 190 nm.

This wavelength region coincides the peak in the excitation spectrum of the 310-nm luminescence band. Thus, the fast scintillation component corresponds to the luminescence band at 310 nm.

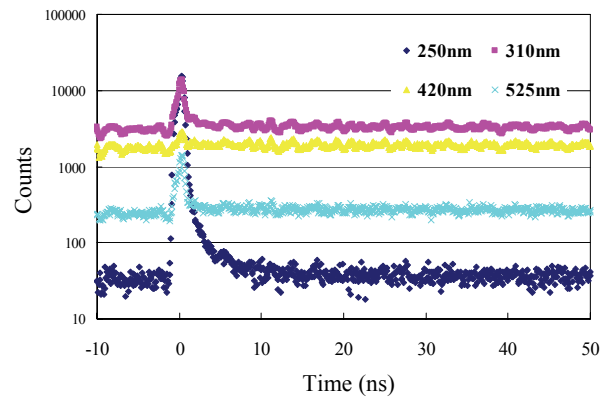


Fig. 1. Luminescence time profiles at various wavelengths under excitation at 158 nm.

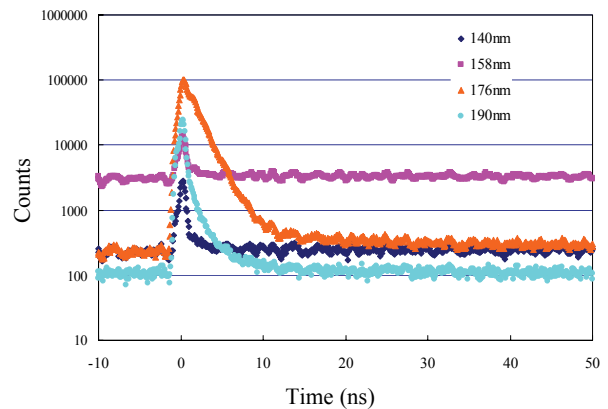


Fig. 2. Luminescence time profiles at 310 nm under VUV excitation at various wavelengths.

[1] M. Koshimizu, K. Onodera, K. Shibuya, H. Saito and K. Asai, *J. Appl. Phys.* **105** (2009) 114912.

[2] M. Koshimizu, K. Onodera and K. Asai, *UVSOR Activity Report* **36** (2009) 119.

[3] K. Onodera, M. Koshimizu and K. Asai, *Radiat. Phys. Chem.* **78** (2009) 1031.

Luminescence Properties of $\text{YBO}_3:\text{Tm}^{3+}$

N. Ohno, K. Tsugawa and K. Kohmoto

*Division of Electronics and Applied Physics, Graduate School of Engineering,
Osaka Electro-Communication University, Neyagawa, Osaka 572-8530, Japan*

Xe dimer (Xe_2) discharge fluorescent lamp is one of the candidates for alternative lighting sources to a conventional Hg discharge fluorescent lamp. New phosphors suitable for the conversion of vacuum ultraviolet (VUV) light into visible light are quite desired at present.

Under the Xe_2 discharge fluorescent excitation, phosphors are excited by VUV light of 7.2 and 8.4 eV. The Hg discharged blue-luminescence phosphor $\text{BAM}:\text{Eu}^{2+}$ ($\text{BaMgAl}_{10}\text{O}_{17}:\text{Eu}^{2+}$) becomes worse in a short time for excitation with VUV light [1]. Therefore, suitable alternative phosphors to $\text{BAM}:\text{Eu}^{2+}$ are necessary under the Xe_2 discharge light excitation. Most rare-earth metal borate hosts are transparent up to 7 - 8 eV, so that the VUV light can directly excite impurity activator in these hosts. The strong absorption due to the impurity ions would give efficient conversion of the VUV light of the Xe_2 discharge lamps [2, 3].

In the present study, luminescence properties of trivalent rare-earth metal ion center in yttrium borate have been studied in the UV and VUV region. The $\text{YBO}_3:\text{Tm}^{3+}$ phosphors were prepared by amounts of the appropriate starting compound powders of Y_2O_3 and H_3BO_3 adding Tm_2O_3 (1 mol %), mixing and firing in a porcelain crucible at 1100°C in the air atmosphere [4]. Impurity Tm^{3+} ions would be expected to be substituted for Y^{3+} ions in the host lattices.

Figure 1 shows luminescence (red curve) and photo-excitation (blue curve) spectra of $\text{YBO}_3:\text{Tm}^{3+}$ measured at room temperature. Luminescence peaks located at 2.3~4.2 eV are observed for the excitation of UV and VUV light. These luminescence lines are attributed to the $f-f$ transitions in Tm^{3+} impurity ions. The blue 2.69 eV line appears strong compared with the case of $\text{YPO}_4:\text{Tm}^{3+}$ phosphor [5]. The relative intensity of these lines would depend on the crystal field around Tm^{3+} ion.

The blue curve in the figure is the excitation spectrum for the 2.69 eV luminescence line. The luminescence of $\text{YBO}_3:\text{Tm}^{3+}$ is effectively excited with 6.1 and 7.2 eV light. These excitation peaks are located at the lower energy than the absorption edge of host YBO_3 (~7.7 eV). The excitation bands at around 6.1 and 6.9 -7.4 eV are ascribed to the $\text{Tm}^{3+} \rightarrow \text{O}^{2-}$ charge transfer transition in Tm^{3+} ions and the $f-d$ transition in Tm^{3+} ion split by the crystal field, respectively. The excitation band higher energy than 7.6 eV is due to the host lattice absorption. The $f-d$ transition energies in Tm^{3+} ions in YBO_3 are found to almost agree with the energy of Xe_2 discharge light.

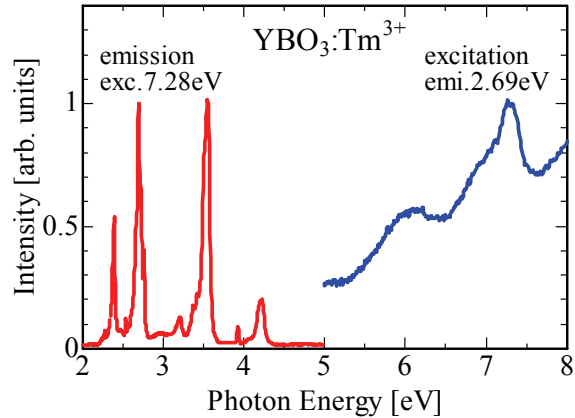


Fig. 1. Luminescence (red curve) and excitation (blue curve) spectra of $\text{YBO}_3:\text{Tm}^{3+}$ at room temperature.

- [1] W. B. Im, H. S. Yoo, S. Vaidyanathan, K. H. Kwon, H. J. Park, Y. I. Kim and D. Y. Jeon, *Mater. Chem. Phys.* **115** (2009) 161.
- [2] H. H. Lin, H. B. Liang, B. Han, J. P. Zhong, Q. Su, P. Dorenbos, M. D. Birowosuto, G. B. Zhang, Y. B. Fu, and W. Q. Wu, *Phys. Rev. B* **76** (2007) 035117.
- [3] N. Ohno and K. Kohmoto, *UVSOR Activity Report* **35** (2008) 82.
- [4] X. Z. Zeng, C. H. Yan, L. D. Sun, Z. G. Wei and C. S. Liao, *J. Lumin.* **121** (2006) 1.
- [5] W. Jia, Y. Zhou, D. A. Keszler, J.-Y. Jeong, K. W. Jang and R.S. Meltzer, *phys. stat. sol. (c)* **2** (2005) 48.

Optical Spectroscopy of Nd:Ce:YAG Ceramics and ZnO Thin Films

M. Yamaga, H. Uno, Y. Kubo and N. Kashiwagura

Department of Mathematical and Design Engineering, Gifu University, Gifu 501-1193, Japan

Ceramic lasers with high power density and high resistance to laser damage are very useful for energy conversion system from inexhaustible solar energy to other optical energy. The absorption spectrum of Ce^{3+} ions in $\text{Y}_3\text{Al}_5\text{O}_{12}$ (YAG) ceramics covers the UV and visible ranges (300-550 nm). On the other hand, ZnO thin films are one of transparent conductive oxides for use as electrodes of solar cell and liquid crystal display.

YAG ceramics codoped with 1 mol % Nd^{3+} and 0.05 mol % Ce^{3+} were sintered by Konoshima Chemical Company. ZnO thin films were deposited on a fused silica glass by the DC sputtering method. Optical absorption, luminescence and excitation spectra for these samples were measured using the BL1B beam in the temperature range of 8-300 K.

Figure 1 (a) shows the optical absorption spectrum in Nd:Ce:YAG ceramics. Fairly broad bands below 240 nm are due to the band-to-band transition and the 4f-5d transition of Nd^{3+} because the band-edge in pure YAG crystals is located around 180 nm. The broad absorption bands around 350 and 550 nm are due to the 4f-5f transitions of Ce^{3+} . Excitation below 240 nm in Nd:Ce:YAG ceramics produces several sharp luminescence lines in the visible (400-630 nm) and near-IR ranges, as shown in Fig. 1(b), being due to the transitions from the multiplet $^2F_{5/2}$ and $^4F_{3/2}$ metastable excited states to other multiplets of Nd^{3+} , respectively. The near-UV (354 nm) excitation of Ce^{3+} produces the visible and near-IR luminescence lines of Nd^{3+} , whereas the another 460 nm excitation of Ce^{3+} produces orange-colored broad band of the Ce^{3+} luminescence and only near-IR sharp Nd^{3+} lines with a lack of the visible lines. These results suggest that the energy transfer occurs from Ce^{3+} to Nd^{3+} in YAG ceramics.

Figure 2(a) shows the optical absorption spectrum and the excitation spectrum obtained by monitoring the 540-nm luminescence intensity in Fig. 2(b) for the ZnO thin films. The broad band below 360 nm is due to the band-to-band transition of ZnO. Figure 2(b) shows the luminescence spectra with various excitation wavelengths at 8 K. The band-to-band excitation below 400 nm produces two broad luminescence bands. In the case of the 450 nm excitation, the 440 nm luminescence band disappears and the 560 nm band remains. The form may be intrinsic luminescence (for example, self-trapped exciton), whereas the latter is the luminescence associated with defects (donor/acceptor recombination). The relation between the luminescence and electrical conductivity will be examined.

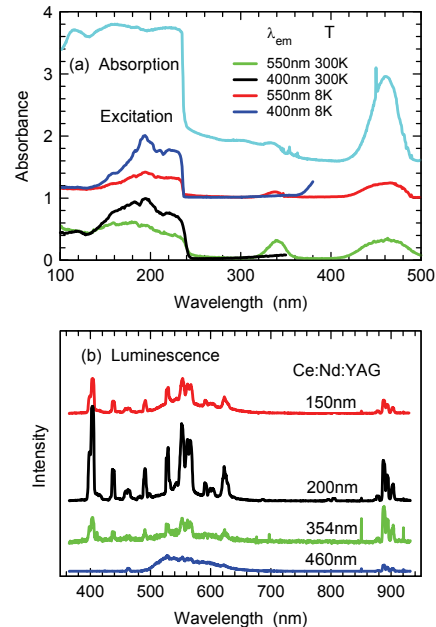


Fig. 1. (a) Absorption/excitation spectra and (b) luminescence spectra in Nd:Ce:YAG ceramics.

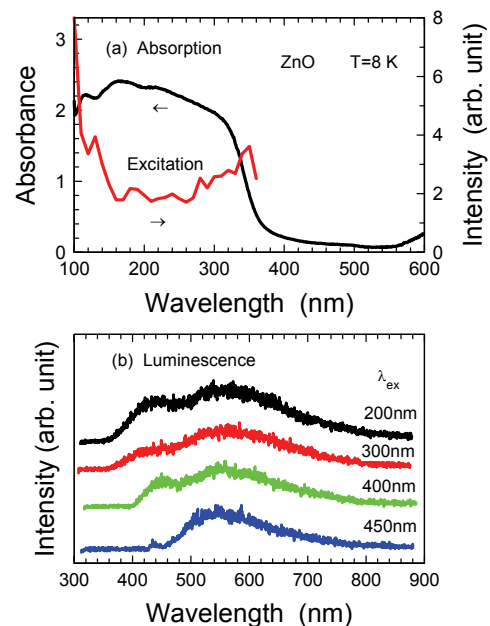


Fig. 2. (a) Absorption/excitation spectra and (b) luminescence spectra in ZnO thin films.

Excitation and Emission Spectra for Nd^{3+} in SrY_2O_4

M. Yoshino¹, Y. Ichikawa¹ and S. Watanabe²

¹ *Department of Materials, Physics and Energy Engineering, Nagoya University, Nagoya 464-8603, Japan*
² *Venture Business Laboratory, Nagoya University, Nagoya 464-8603, Japan*

The trivalent lanthanide ions (e.g. Er^{3+} , Ce^{3+} , Yb^{3+}) in oxide crystals have drawn attentions due to their application for luminescent materials in NIR to UV regions such as solid-state lasers or phosphors. And, Nd^{3+} has also attracted attentions as luminescence centers. In this work, the excitation spectra and emission spectra for Nd^{3+} in SrY_2O_4 crystal have been measured. The Nd doped SrY_2O_4 samples are produced by solid state reactions in 1373 K. The concentration of Nd^{3+} in the sample is 3 mol%. The emission spectrum for Nd^{3+} in SrY_2O_4 at 200 nm excitation is shown in Fig. 1. The broad peak appearing below 400 nm and the sharp peaks appearing around 400-600 nm are expected to relate to the emission of SrY_2O_4 host and Nd^{3+} 4f-4f

transition, respectively. The excitation spectrum monitored at 334 nm emission is shown in Fig. 2. The peak near 200 nm corresponds with that in the spectrum monitored at 423 nm in SrY_2O_4 host [1], and it relates to the absorption from the optical transition around the band edge in SrY_2O_4 . On the other hand, the peaks are measured around 230-250 nm in the excitation spectrum monitored at 555 nm emission (Fig. 3). These peaks are due to the Nd^{3+} 4f-5d transition. Then, in the excitation at 230 nm, Nd^{3+} ions are excited directly, the emission spectrum mainly shows the sharp peaks originated from Nd^{3+} 4f-4f transition (Fig. 4).

[1] M. Yoshino, S. Watanabe and Y. Ichikawa, UVSOR Activity Report 36 (2009) 122.

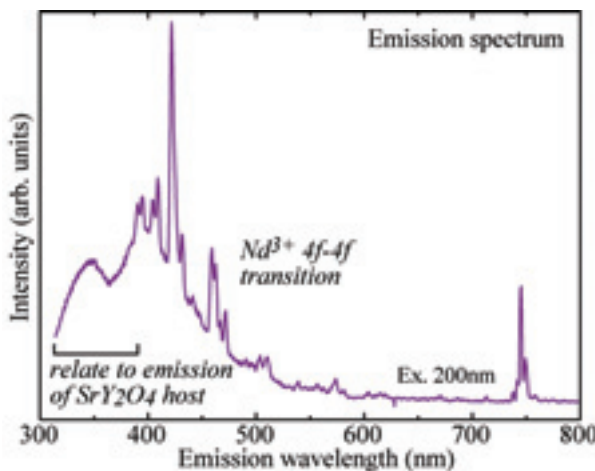


Fig. 1. Emission spectrum for Nd^{3+} in SrY_2O_4 .

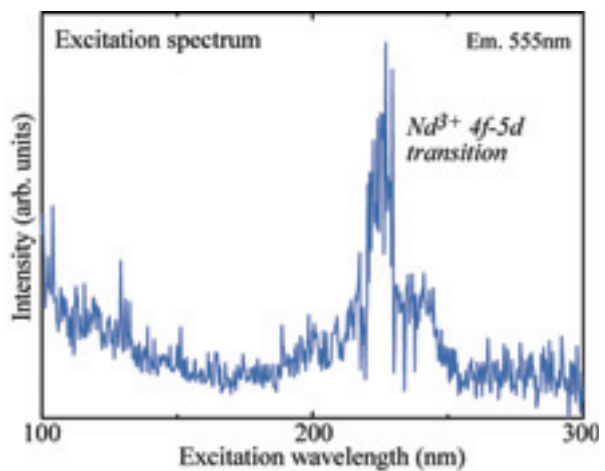


Fig. 3. Excitation spectrum for Nd^{3+} in SrY_2O_4 .

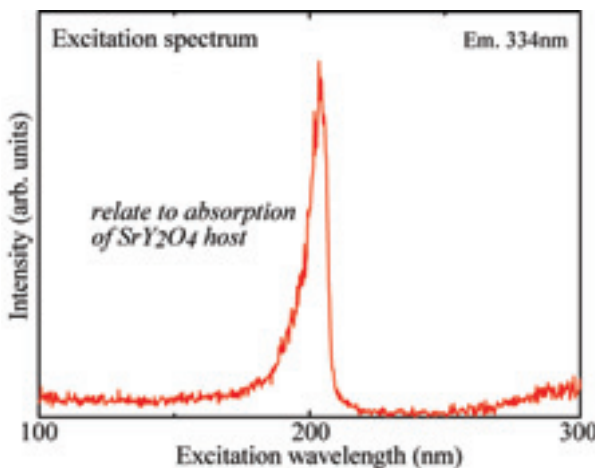


Fig. 2. Excitation spectrum for Nd^{3+} in SrY_2O_4 .

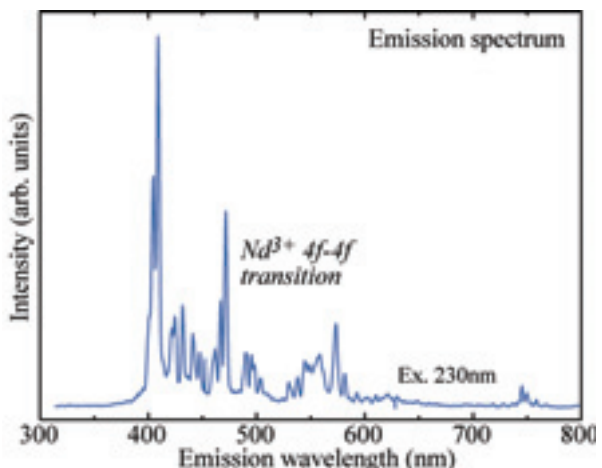


Fig. 4. Emission spectrum for Nd^{3+} in SrY_2O_4 .

Electronic Structural Changes of Electrochemically Oxidized $\text{Li}_{2-x}\text{CuO}_2$

Y. Arachi, K. Hinoshita and Y. Higuchi

Department of Chemistry, Materials Engineering, Kansai University, Osaka 564-8680, Japan

New potential cathode materials to replace LiCoO_2 are under extensive investigation. Among them, we focus on copper because of its abundant resources and the less toxicity. Additionally, higher cell potential can be expected in view of its electronic structure composed of trivalent Cu and O. Electrochemical study of Li_2CuO_2 was reported that a rechargeable capacity of 130 mAhg^{-1} was obtained with an average voltage of 2.5 V although it has 490 mAhg^{-1} of theoretical capacity[1]. In this study, using experimental and ab-initio calculation results we investigate the changes in electronic structure of Li_2CuO_2 caused by Li-de/intercalation electrochemically and discuss the possibility of cathode material with high energy density.

The conventional solid-state reaction was used. Starting materials were composed of chemical grade Li_2CO_3 and CuO . After mixing them properly, pellets were made by the pressing. Then, they were calcinated at 1023 K for 24 h and sintered at 1073 K for 24 h. De-lithiated samples were electrochemically prepared using coin-type cells with $\text{Li}/1\text{M LiClO}_4$ in $\text{PC}:\text{DMC}(1:1)$ /samples. X-ray absorption measurements of above samples at the Cu L - and O K -edges by the total electron yield were performed on BL4B and (UVSOR-II, Okazaki, Japan). The first principle calculations were carried out using the WIEN2k program package, which is based on the full potential augmented plane wave and local orbitals (APW+lo) method within the generalized gradient approximation (GGA). The maximum wavelength of APW, K_{max} , was determined to satisfy the condition of $R \times K_{\text{max}} = 7$, where R is the muffin-tin radius of the O atom. The warped electron density in the interstitial region was described by a finite Fourier series with maximum wave vector, G_{max} , where G_{max} satisfies 12. The maximum angular momentum l for partial spherical waves inside atomic spheres was 10. A mesh $10 \times 10 \times 10$ over the irreducible Brillouin zone was used, producing 224 inequivalent k -points.

Figure 1 shows that the results of a first principle calculation for Li_2CuO_2 and LiCuO_2 . It clearly indicates a difference between them, specifically in a valence band state distribution of oxygen. A considerable electron loss of oxygen was occurred by Li-extraction. Figure 2 shows XANES spectra of O K -edges for Li_2CuO_2 and electrochemically Li-deintercalated $\text{Li}_{2-x}\text{CuO}_2$ at various voltages. On the basis of these results, we will examine the role of oxygen during charging reaction at higher voltage region.

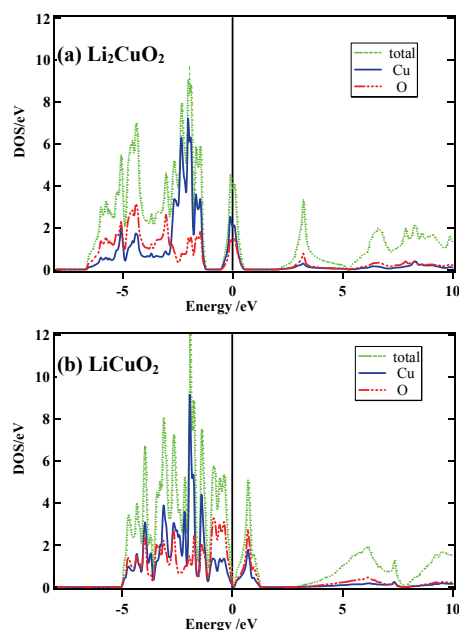


Fig. 1. Density of State for (a) Li_2CuO_2 and (b) LiCuO_2 .

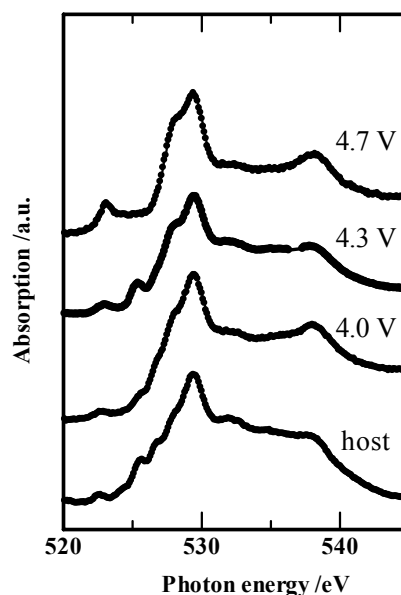


Fig. 2. O K -edge XANES of electrochemically oxidized $\text{Li}_{2-x}\text{CuO}_2$.

- [1] H. Arai *et al.*, *Solid State Ionics* **106** (1998) 45.
 [2] A. S. Prakash *et al.*, *Chem. Mater.* **17** (2005) 4406.

Effect of Periodicity Fluctuations on Mini-Band Structure in Strained Superlattice Semiconductor

T. Ujihara¹, K. Hashimoto¹, Y. Maeda¹, H. Miyazaki³, M. Kuwabara² and Y. Takeda¹

¹Graduate School of Engineering, Nagoya University, Nagoya 464-8603, Japan

²Graduate School of Science, Nagoya University, Nagoya 464-8602, Japan

³UVSOR Facility, Institute for Molecular Science, Okazaki 444-8585, Japan

Recently, a quantum dot solar cell is proposed to achieve a high conversion efficiency. The concept of the quantum dot solar cell is to utilize mini-bands in the periodic alignment of quantum dots, as middle band in the carrier excitation in order that the band structure is matched the solar light spectrum. The theoretical calculation indicates that the conversion efficiency can reach over 50% assuming "the perfectly periodic potential." However, it is presently impossible to produce quantum dots, of equal size, periodically.

In this study, the effect of periodicity fluctuation on the mini-band structure was investigated from the viewpoint of the followings: (1) the effect on energy and band width of the mini-band structure, (2) the effect on the conduction and lifetime of carriers in the mini-band. In place of quantum dot alignment, we examined the superlattice structure based on multiple quantum well of which the preparation method has been established.

We prepared the InGaAs/GaAs superlattice structures as shown in Fig. 1. On the structure with the periodicity fluctuation, the film thickness of one well layer of the superlattice structure was made thicker. On the evaluation of the mini-band structure, the synchrotron-radiation photoemission measurements at BL-5U of the UVSOR facility were scheduled. (However, we could measure only the GaAs bulk crystal as the preliminary experiment in the present study.) In addition, the quantum efficiency measurement was carried out as an evaluation of electronic conduction in the mini-band. In this study, the quantum efficiency was evaluated by measuring the current due to the electrons taken out from the conduction band to the vacuum via the NEA surface.

Figure 2 shows the angle-resolved photoemission mapping of GaAs bulk crystal. θ is the tilt angle from [001] to [110]. There are mainly three bands in this mapping profile. Since these band structures are symmetrical for the angle at around 1 deg, this symmetry center seems to be the Γ point of GaAs. Figure 2(b) is the spectrum mapping measured by changing the energy of incident beam. The symmetry around Γ point is also observed. From this mapping, the inner potential was determined to be around 50 eV. This value is useful for the measurement of superlattice mini-bands in future.

Figure 3 is the quantum efficiency spectrum as a

function of wavelength of excitation laser light. In the case of the sample without the periodicity fluctuation, the photocurrent was detected from 700 nm to over 1000 nm, and the spectrum was a step for the wavelength. The stepped spectrum reflects a density of state of superlattice structure. In the case of the sample with the periodicity fluctuation, the quantum efficiency decreases by 10^{-1} – 10^{-3} comparing that without the fluctuation. It is serious for the solar cell properties that the fluctuation of only one well layer thickness largely decreases the quantum efficiency.

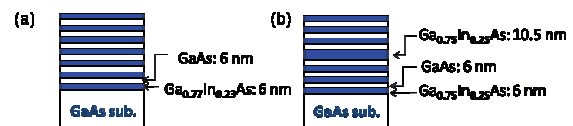


Fig. 1. Sample structures of (a) superlattice without periodicity fluctuation and (b) superlattice with periodicity fluctuation.

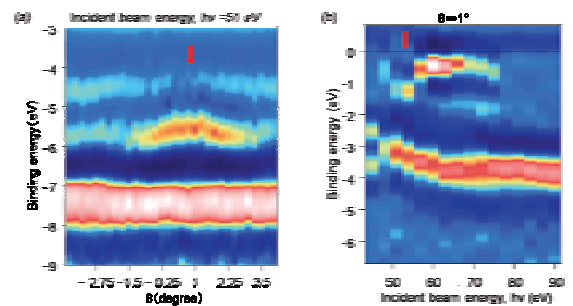


Fig. 2. Photoemission spectra mapping from GaAs bulk crystal: (a) Angle-resolved photoemission mapping and (b) Photoemission mapping as a function of incident beam energy.

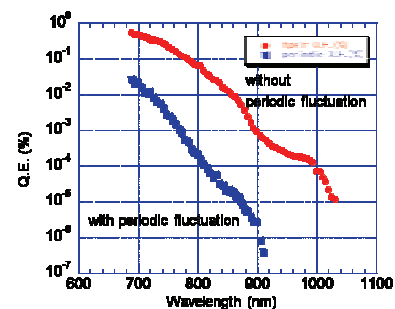


Fig. 3. Quantum efficiency as a function of wavelength of excitation light.

Observation of Photodegradation in Amorphous Semiconductors by Ultraviolet Synchrotron Orbital Radiation

K. Hayashi

Department of Electrical and Electronic Engineering, Gifu University, Gifu 501-1193, Japan

Introduction

The time-dependent change in photoconductivity during and after irradiation of bandgap (BG) light has been observed in many amorphous semiconductor materials. [1] This phenomenon usually called photodegradation and is explained in terms of the creation of photoinduced metastable defects. In device application of these materials, the creation of those defects is serious problem. The photodarkening is also a well-known phenomenon in amorphous chalcogenide materials. The photodarkening is a parallel shift to the optical absorption edge to lower energy side after irradiation of BG light. This darkened state is removed by annealing near the glass-transition temperature. The x-ray diffraction and the volume change of the films before and after irradiation of BG light suggest that photodarkening is due to a change of the local structure of the amorphous network.[2] Although many models are proposed for the creation of those defects and the photodarkening, details of the microscopic mechanism are still not clear. Understanding the physical mechanism metastability is one of the important fundamental problems associated with these materials.

The measurement of the total photoelectron yield (TPY) at the vacuum ultra-violet region is a powerful tool for the study of the energy structure. TPY will reflect the optical absorption and the photoconductivity of the material. In this report, we investigate photoinduced phenomena by measuring TPY of amorphous films.

Experimental

Thin films of amorphous materials (a-As₂S₃ and a-Si) were prepared onto quartz substrates which fabricated Au electrodes by conventional evaporation technique. The thickness of the amorphous films was from around 160nm to 300nm. The samples were annealed at appropriate temperature (443K for a-As₂S₃ and 473K for a-Si) for two hours in a vacuum. A xenon arc lamp with IR-cut-off filter was used as a BG light source. The measurements of TPY were performed at room temperature at the BL5B beam line. For a-As₂S₃, the VUV probe light to measure TPY was fixed to the wavelength that was able to excite 3d core level of As atom. For a-Si, the VUV probe light was fixed to the wavelength that was able to excite 2p core level of Si atom. A pinhole of 1.5mm in a diameter was inserted between the monochromator and sample to remove stray light. The intensity of the VUV probe light was monitored

by measuring TPY of two Au meshes.

Results and Discussion

Figure 1 shows examples of the time-dependent change in TPY of a-As₂S₃ and a-Si films by irradiation of BG light. This figure is obtained by TPY normalized by the initial value of the measurement. As shown in the figure, during irradiation of BG light, TPY of a-As₂S₃ is gradually increased and it seems to be finally saturated.[3] On the other hand, TPY of a-Si doesn't depend on the presence of irradiation of BG light, and decreased monotonously. It seems that the difference of the TPY change in both samples is related whether to cause the photodarkening. The photodarkening only is observed in amorphous chalcogenide materials, and not observed in a-Si. In a-Si film, since defects are also generated by irradiation of high energy photons [4], it is thought that TPY was decreased by the creation of defects dominantly induced by the VUV probe light. However, it doesn't understand that a decrease of TPY by the photodegradation is not observed in a-As₂S₃ at present. The relation among this TPY change, the photodegradation, and the photodarkening will be more clarified in the next step.

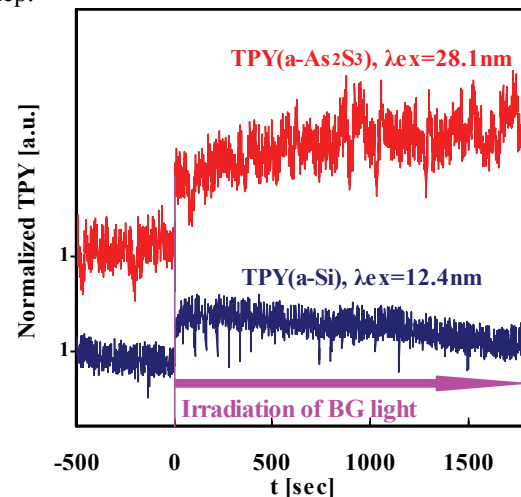


Fig. 1. The photoinduced change of TPY by irradiation of bandgap light in a-As₂S₃ and a-Si films.

References

- [1] D. L. Staebler and C. R. Wronski, *Appl. Phys. Lett.* **31** (1977) 292.
- [2] Ke. Tanaka, *Rev. Solid State Sci.* **4** (1990) 641.
- [3] K. Hayashi, *UVSOR Activity Report* **36** (2009)125.
- [4] Pontuschka *et al.*, *Phys. Rev. B.* **25** (1982) 4362.

Characterization of Novel TiO₂/ZnO Multilayer Mirrors at "Water-Window" Wavelengths

Y H. Kumagai¹, Y. Tanaka¹, M. Murata¹, T. Shinagawa² and A. Kobayashi¹

¹Graduate School of Engineering, Osaka City University, Osaka 558-8585, Japan

²Inorganic Materials Lab., Osaka Municipal Technical Research Institute, Osaka 536-8553, Japan

Development of high-performance normal-incidence multilayer optics for the water-window wavelength region between the oxygen and carbon K absorption edges at 2.33 and 4.36 nm, respectively, where water is relatively transmissive and organic materials are absorptive, has been a technical challenge of great interest. The extremely small periods (1.2-2.2 nm) of soft-x-ray reflectors require very rigorous specifications to be met with respect to interface roughness and interlayer mixing, because interface roughness on an atomic scale has a substantial effect on soft-x-ray reflectance. Therefore, the highest reflectance achieved at water-window wavelengths ($\lambda=3.18$ nm) and near normal incidence ($\theta=9^\circ$) has been 3.3% at the first half of 1990's [1], in spite of the various efforts which have been made in this field. The reason that the reflectances achieved at these wavelengths are so low is that the Fresnel coefficients of materials are so small at these wavelengths that a large number of bilayers must be used, which means that the problems of interface roughness and imperfect interfaces due to interlayer mixing become serious.

The authors have proposed the use of a novel metal oxide multilayer for soft-x-ray reflectors at water-window wavelengths, because an oxide multilayer can prevent the formation of an alloy at the interface without any diffusion barrier, and the absorption of oxygen in oxides is negligible at the water-window wavelengths; moreover, the metal oxide multilayer can be fabricated by the atomic layer deposition or atomic layer epitaxy technique. These techniques can be used to control surfaces on an atomic scale by sequentially dosing the surface with appropriate chemical precursors and then promoting surface chemical reactions which are inherently self-limiting. We have found that the self-limiting adsorption mechanism works in the fabrication of oxide thin films such as aluminum oxide and titanium oxide [2]. And we reported that we have experimentally demonstrated high reflectance of over 30% at a wavelength of 2.734 nm and an incident angle of 71.8° from the normal incidence using novel metal oxide multilayers of titanium oxide and aluminum oxide fabricated by the atomic layer deposition method of controlled growth with sequential surface chemical reactions. For x-ray processing, crystalline multilayer mirrors might be rather useful than amorphous ones. Therefore, in this study, the authors demonstrated that novel oxide superlattice structures of crystalline TiO₂/ZnO on

sapphire substrates were fabricated for high-reflection multilayer mirrors at 2.734 nm. Theoretical calculations also indicated that these structures could give high reflectance over 50% at the wavelength. In the experimental study, both rutile TiO₂ (200) and wurtzite ZnO (0001) thin films were grown epitaxially on the same sapphire (0001) substrates by atomic layer epitaxy (ALE) at 450°C. We demonstrated for the first time that the novel oxide superlattice structure of 10-bilayer TiO₂/ZnO on a sapphire substrate gave high reflectance of 29.4% at a wavelength of 2.734 nm, as shown in Fig. 1.

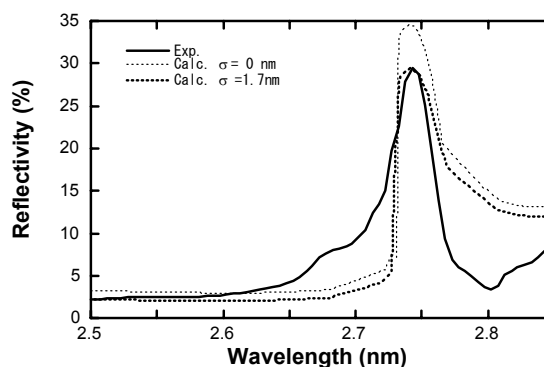


Fig. 1. Experimental reflectances of the ALE-grown 10-bilayer ZnO/ TiO₂ structure on a sapphire (0001) substrate. $\theta=85^\circ$.

[1] I. V. Kozhevnikov, A. I. Fedorenko, V. V. Kondratenko, Yu. P. Pershin, S. A. Yulin, E. N. Zubarev, H. A. Padmore, K. C. Cheung, G. E. van Dorssen, M. Roper, L. L. Balakireva, R. V. Serov and A. V. Vinogradov, Nucl. Instrum. Methods Phys. Res. A **345** (1994) 594.

[2] H. Kumagai, K. Toyoda, K. Kobayashi, M. Obara and Y. Iimura, Appl. Phys. Lett. **70** (1997) 2338.

Far-Infrared Reflective Study of Li-Doped Alkali Niobate System

H. Matsudo, Y. Shikai, S. Tachi, I. Kagomiya and K. Kakimoto

Graduate School of Engineering, Nagoya Institute of Technology, Nagoya 466-8555, Japan

Alkali niobate oxide is one of the lead-free piezoelectric materials. The electrical property varies with alkali component, especially with the density of Li ion. In our previous study at BL6B[1], the absorption of Na and K ion translational modes of $\text{Li}_{0.06}(\text{Na}_{0.5}\text{K}_{0.5})_{0.94}\text{NbO}_3$ (LNKN06) were not clear and the softening of the translational modes was not observed between the spectrum at 78 K and that at 300 K in spite that the phase transition from rhombohedral to orthorhombic crystal structure exists at 270 K. In this study, IR reflectivity of LNKN06 and NKN ceramics were measured to clarify the effect of Li incorporation against the lattice vibration around NbO_6 octahedral unit in perovskite structure.

Reflectivity far-infrared spectra of $\text{Na}_{0.5}\text{K}_{0.5}\text{NbO}_3$ (NKN) and LNKN6 ceramic samples were obtained at the range from 78 to 313 K at the BL6B beam line of UVSOR. The spectra were corrected by using Michelson interferometer (Bruker, IFS66v) and synchrotron radiation source.

Figure 1 shows far-infrared reflectivity spectra of NKN ceramics. Broad absorption was observed from 150 to 200 cm^{-1} that attributed by TO phonon of the vibration of Na and K ions against the NbO_6 octahedral unit. The spectra clearly show the phase transition from rhombohedral to orthorhombic crystal structure between 78 and 100 K on heating process. This reflects that the phase transition of NKN includes the softening of translational modes of Na and K ions.

On the other hand, the far-infrared reflectivity spectra of LNKN06 are not changed around at 273K, at which the LNKN06 ceramics shows orthorhombic to tetragonal phase transition. However, there is several absorption band ranging from 120 to 300 cm^{-1} .

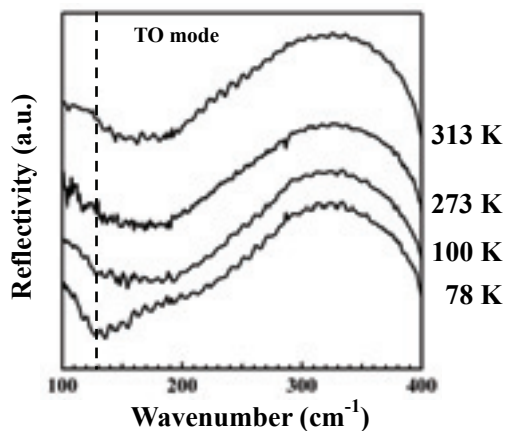


Fig. 1. Far-infrared reflectivity spectra of NKN ceramics at the range 78 to 313 K.

The real part of dielectric permittivity of NKN and LNKN ceramics at 273K, which were calculated from reflectivity by Kramers-Kronig relation, shows the difference around 200 cm^{-1} . This result indicates that the distortion of NbO_6 was induced by the small ion of Li in NKN perovskite structure, which corresponds to our previous study by Raman spectroscopy[2].

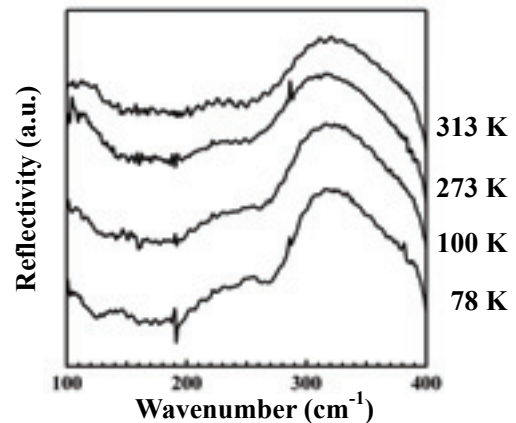


Fig. 2. Far-infrared reflectivity spectra of LNKN06 ceramics at the range 78 to 313 K.

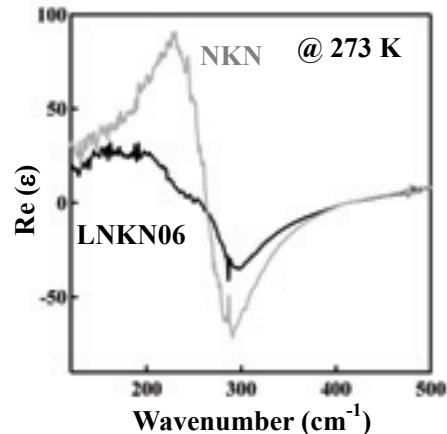


Fig. 3. The real part of dielectric permittivity of NKN and LNKN06 ceramics at 273K.

Acknowledgement

This research was supported by the Industrial Technology Research Grant Program in 2007 from the New Energy and Industrial Technology Development Organization (NEDO) of Japan

References

- [1] H. Matsudo, Y. Inagaki, T. Sumi, I. Kagomiya and K. Kakimoto, UVSOR Activity Report **36**(2009) 128.
- [2] T. Hotta, K. Kakimoto and H. Ohsato, Key Eng. Mater., **368-372** (2008) 1893.

Reflectivity Spectra of SrGa₂S₄ Crystals

M. Kitaura¹, A. Ohnishi¹, M. Sasaki¹ and M. Itoh²

¹Department of Physics, Yamagata University, Yamagata 990-8560, Japan

²Department of Electrical and Electronics Engineering, Shinshu University, Nagano 380-8553, Japan

Alkaline-earth thiogallates are known to be host materials of thin-film electroluminescence (EL) phosphors. The EL phenomena in inorganic phosphors originate from the creation of hot electrons by high electric field, but the excitation mechanism of luminescence centers still remains open in rare-earth doped alkaline-earth thiogallates. One of the reasons is that there are few studies on the electronic structures of them. Since the behavior of hot carriers reflects the valence and conduction bands, the electronic structure of host materials is of great importance in order to clarify the excitation mechanism of luminescence centers. In the present study, we have investigated the electronic structure of strontium thiogallate SrGa₂S₄ by the measurement of reflectivity and X-ray photoelectron spectroscopy (XPS) spectra and the cluster calculation based on the relativistic discrete variational X α (DV-X α) method [2].

The crystals of SrGa₂S₄ were grown by a chemical vapor transport method. A small amount of iodine was used as a transport agent. Our samples have high-quality surface for the crystalline *ac* plane, the average size of which was 3×0.5×2 mm³. From the X-ray diffraction measurement, it turns out that they have the structure of SrGa₂S₄. Reflectivity spectra of them were measured at the BL7B beam line of UVSOR. Optical constants were calculated by the Kramers-Kronig transformation of reflectivity.

Figure 1 shows the typical absorption spectrum of SrGa₂S₄ in the 3–30 eV energy range at 300 K. The first increase in absorption coefficient occurs at 4.34 eV, and a prominent peak appears at 5.36 eV. As the photon energy is increased, the second increase takes place around 9.5 eV, which is followed by a broad structure in the high-energy side.

The partial density of states (PDOS) curves for a number of atomic orbitals of Sr, Ga, S are shown in Fig. 2. The zero energy is set to the top of the valence band. The valence band (VB) is dominated by S 3p orbitals, the full base width of which is 6 eV in rough estimation. This value is in good agreement with the VB width estimated from XPS spectra. The conduction band (CB) is mainly composed of 4d orbitals of Sr in the lower part and p orbitals of Sr and Ga in the upper part.

From the PDOS curves of Fig. 2, the electronic transition from the VB of S 3p to the lower CB of Sr 4d is expected in the lowest energy position. Thus, we assign the 5.36 eV absorption peak to the VB → lower CB transition. In the high-energy position,

since the large joint density of states is expected for the transitions from the VB to the upper CB of Sr 5p + Ga 4p, the broad structure above 9.5 eV is assigned to the transition from the VB to the upper CB.

We found a number of fine structures in the absorption spectra at around 10 K. These structures showed remarkable dichroism. An analysis for the polarization dependence of absorption spectra is now in progress.

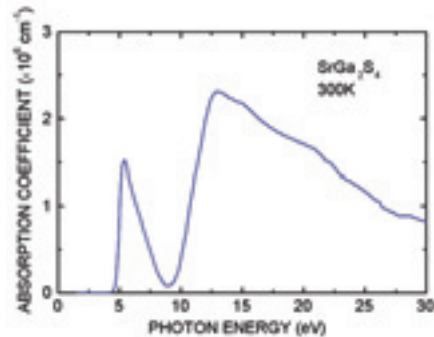


Fig. 1. Absorption spectrum of SrGa₂S₄ crystal at 300 K calculated by the Kramers-Kronig analysis.

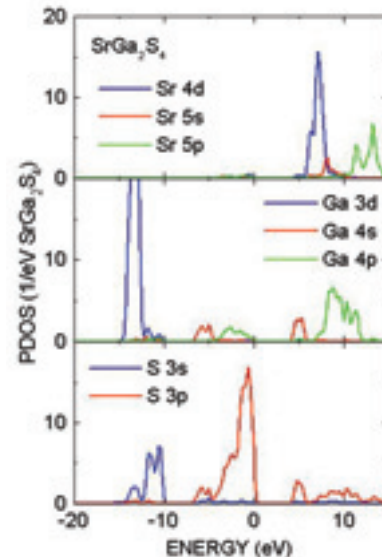


Fig. 2. Partial density of states curves of SrGa₂S₄. The zero energy was set to the top of the valence band.

[1] M. Yoshida, A. Mikami and T. Inoguchi: in *Phosphor Handbook*, ed. S. Shionoya and W. M. Yen (CRC Press, Boca Raton, FL, 1999) p. 581.

[2] H. Adachi, M. Tsukada and C. Satoko, *J. Phys. Soc. Jpn.* **45** (1978) 875.

Azo Dyes as Photosensitizers for Organic Solar Cells

K. Nakajima^{1,2}, K. Ohta¹, H. Katayanagi^{2,3} and K. Mitsuke^{2,3}

¹Science Research Center, Hosei University, Tokyo 102-8160, Japan

²Institute for Molecular Science, Okazaki 444-8585, Japan

³Graduate University for Advanced Studies, Okazaki 444-8585, Japan

The dye sensitized solar cell (DSC) has attracted universal attention because of its high-solar-energy-to-electricity conversion efficiency and relatively low cost of its manufacturing [1]. Panchromatic sensitizers which can efficiently absorb the sunlight are in the stage of research and development. So far the best photovoltaic performance has been achieved with ruthenium complex dyes, but organic dyes have also stimulated intensive research efforts [2]. In the present study, we focused our attention on azo compounds which have been widely used for dyes and pigments with excellent lightfastness. The main advantage of azo dyes is their facile introduction of various substituents onto the main structure R-N=N-R', permitting us to easily modify their electronic and spectroscopic properties.

We designed various azo dyes having carboxylate and hydroxy groups whose positions and numbers differ from one dye to another. We synthesized 25 azo dyes and compared their performance among nine azo dyes that have the same basic structure (naphthyl-azo-benzene). Titanium dioxide paste (PST-18NR: Shokubaikasei kogyo) was applied on the FTO glass (Asahi glass) by screen printing, and sintered at 450°C for 30 min. After adsorption of an azo dye, electrolyte solution (AN-50: Solaronix Inc) was dropped on the titania electrode which was combined with a counter electrode glass covered with Pt.

Photovoltaic measurements of the DSCs thus fabricated were performed using a solar simulator

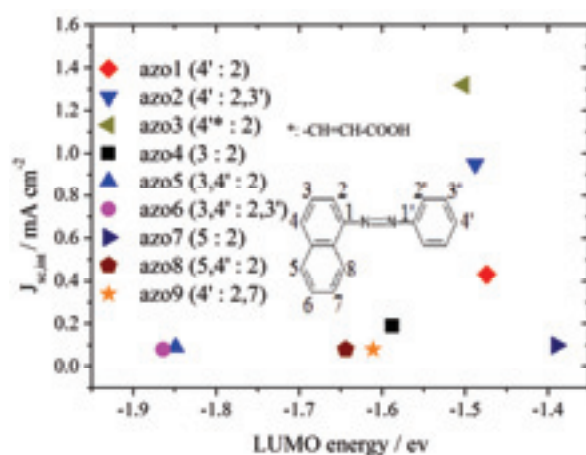


Fig. 1. Correlation between the experimental data of the short current density of DSCs and the theoretical LUMO energy levels of the solitary azo dyes. The positions of carboxylate and hydroxy groups are shown using the numbers before and after the semicolon in the parentheses, respectively.

equipped with a xenon lamp (Peccell Technologies, PEC-L11). Figure 1 shows a plot of the short current density $J_{SC,int}$ vs LUMO energy among 9 DSCs. The LUMO energies were estimated by using MOPAC7 for the semiempirical quantum chemistry program. There is a salient correlation between $J_{SC,int}$ and the LUMO energies, that is, the three dyes with the LUMO energies of ca. -1.5eV give higher $J_{SC,int}$ than the other dyes having the energies of < -1.5 eV. This observation suggests that the performance of the present DSCs is dominated crucially by the quantum yield of the electron injection from the excited dyes. An only exception is DSC made of azo7 whose calculated LUMO level is as high as -1.390 eV. Explanation for the low-performance of the DSC with azo7 might be its possible incompatibility with AN-50. When homemade redox electrolyte solution was employed in place of AN-50, $J_{SC,int}$ for azo7 was found to be improved and become almost comparable with that for azo2.

The optical densities of dye molecules adsorbed on TiO₂ can be evaluated from $\log_{10}(I_{blank}/I_{cell})$, where I_{blank} and I_{cell} are the intensities of the transmitted BL7B synchrotron radiation through a blank cell and a DSC, respectively, in addition to the measurement of J_{sc} . The quantum yield Y_{inj} for electron injection from the excited dye to TiO₂ can be evaluated by using these data [3], and are shown in Fig. 2.

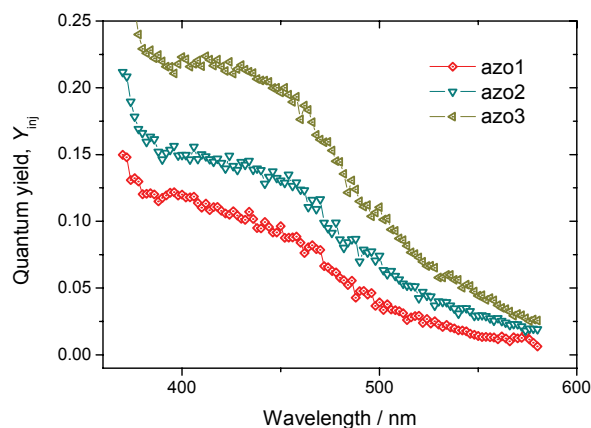


Fig. 2. Approximate quantum yields for electron injection from the excited level of the dyes.

[1] B. O'Regan and M. Grätzel, *Nature* **353** (1991) 737.

[2] Y. Ooyama and Y. Harima, *Eur. J. Org. Chem.* **2009** (2009) 2903.

[3] K. Nakajima, *et al.*, in the Proceedings of Pure and Applied Chemistry International Conference 2010 (PACCON 2010), Thailand, PTC-PO-19.

Local Environment Analysis of P Atoms in Proton-Conducting Amorphous Zirconium Phosphate Thin Films

Y. Aoki, K. Ogawa and H. Habazaki

Graduate School of Engineering, Hokkaido University, N13W8, Sapporo 060-8628, Japan

Previously, we reported that amorphous zirconium phosphate thin films exhibit the enhanced proton conductivity in nonhumidified atmosphere in the intermediate temperature range [1]. This superior conductivity is speculated to be related to the structure of phosphate groups. Here, we identify the phosphate species in amorphous zirconium phosphate thin film by P L-edge XAS.

The amorphous zirconium phosphate, α -ZrP_{2.5}O_x, films were prepared on an ITO substrate (Aldrich) by multiple spin-coating of precursor solutions of tetrabutoxyzirconium (Zr(O^tBu)₄) (Kanto) and phosphorous oxide (P₂O₅) (Kanto) at the Zr/P atomic ratio of 1/3. The details of the procedure were described elsewhere [1]. The metal concentration (Zr+P) in the precursor mixture sol was adjusted in 50 mM. The precursor sols were spin-coated onto the ITO substrate at 3000 rpm for 40 sec by a Mikasa 1H-D7 spin coater. The deposited gel layer was hydrolyzed by blowing hot air for 30 sec (Iuchi hot gun), and the substrate was cooled to room temperature by blowing cold air for 20 sec. These cycles of spin-coating, hydrolysis and cooling were repeated 10-20 times and the gel film thus obtained was calcined at 400°C for 30 min. The combination of deposition and calcination was repeated more than 3 times, and the final calcination was performed at 450°C for 2 h. The hydrated films were prepared by heating them at 450°C for 12 h in H₂O/air ($p_{\text{H}_2\text{O}} = 4.2$ kPa).

P L-edge XAS spectroscopy was carried out with α -ZrP_{2.5}O_x films of 40 nm, 55 nm, 100 nm and 300 nm-thickness (Figure 1). It is reported that P L-edge spectra of inorganic phosphate salts is very sensitive to the polymerization degree, n , of phosphate group P_nO_{3n+1}[2]. Here, the Zr(HPO₄)₂ was used as a reference material of orthophosphate configuration and ZrP₂O₇ as that of pyrophosphate configuration, respectively. The P L-edge spectra of zirconium phosphates was composed of the several peaks in agreement with those of the other phosphate compounds, which are assigned largely to the transition from P core level to unoccupied states. Peaks C and C' appear at around 139 eV and 141 eV, respectively, and are assigned to the transition of P 2p electron to 3p-like t₂ states. Peak D at around 148 eV is attributed to the transition 3d-like e states. Peak A is assigned to the transition of P 2p electron to 3s-like a₁ states and splits into two peaks of A' and A by spin-orbit interaction of P 2p orbitals. Yin et al reported that the peaks A and A' in P L-edge spectra rapidly shift to high energy from orthophosphate to pyrophosphate to metaphosphate and peak A of

Na₃PO₄, Na₄P₂O₇ and Na₅P₃O₁₀ appears at 135.35, 135.85 and 135.96 eV, respectively [2]. Peak A' in zirconium phosphates is very weak to appear as a shoulder. Peak A appears at 136.3 eV for ZrH₂(PO₄)₂ and at 136.7 eV for ZrP₂O₇. P L-edge spectra of dry α -ZrP_{2.5}O_x films are very similar for all thicknesses and the peak A appears at 136.8 ± 0.07 eV. This value is very close to the peak A of ZrP₂O₇. Furthermore, the spectral features of hydrated α -ZrP_{2.5}O_x films are almost same as those of the dry films. These results indicate that the pyrophosphate is predominant form of phosphate group in the films even though they are as-prepared or hydrated at elevated temperatures.

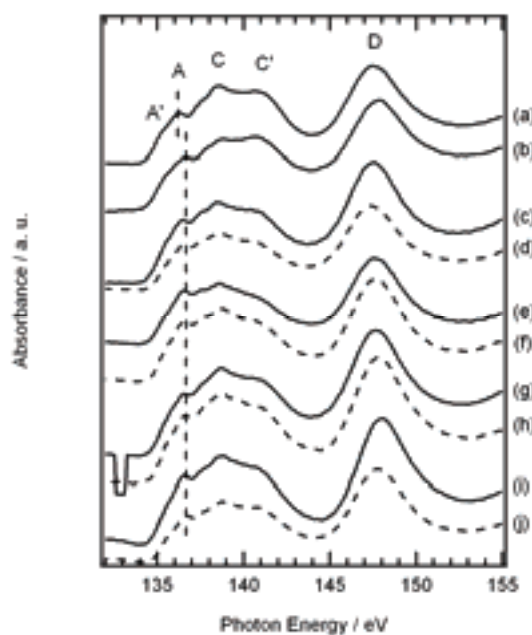


Fig. 1. P L-edge XANES spectra of (a) Zr(HPO₄)₂ and (b) ZrP₂O₇, and amorphous ZrP_{2.5}O_x films with thickness of (c), (d) 40 nm, (e), (f) 55 nm, (g), (h) 100 nm and (i), (j) 300 nm. Solid line indicates as-prepared film and dashed line hydrated film.

[1] Y. Li *et al.*, Adv. Mater. **20** (2008) 2398.

[2] Z. Yin *et al.*, Phys. Rev. B **51** (1995) 742.

N K-Edge XANES Analysis of Nitrogen Doped TiO₂ Photocatalyst

T. Yoshida¹, S. Muto¹ and E. Kuda²

¹*EcoTopia Science Institute, Nagoya University, Nagoya 464-8603, Japan*

²*Department of Materials, Physics and Energy Engineering, Nagoya University, Nagoya 464-8603, Japan*

Introduction

In the field of catalytic chemistry, a specific function in a solid catalyst crucially depends on the chemical state of a specific active component (active site). In this context X-ray absorption fine structure (XAFS) and electron energy loss spectroscopy (EELS) are expected as one of the most powerful techniques for chemical state analysis of the active site, because they provide information on the local structure and electronic states around the specific element of interest. The purpose of the present study is to examine the local chemical states of nitrogen injected into TiO₂ photocatalysis by means of a sophisticated combination of XAFS and EELS. The nitrogen doped TiO₂ has been attracting much attention due to its visible-light response to natural solar light.

Experimental

The samples used in this study were TiO₂ (1 0 0) single crystals (5 x 5 x 0.5 mm³), supplied by Furuuchi Kagaku, Japan. Mass analyzed 100 keV N₂⁺ ions (50 keV/N⁺ ion) were injected into the samples at room temperature, perpendicular to the sample surface. The N⁺ fluence ranged from 1 to 5 x 10²¹ m⁻². After the ion implantation, parts of the samples were heat-treated at 573 K for 2 hours in air.

N K-edge XANES spectra of the N⁺-implanted TiO₂ samples were measured at the BL-8B1 station of UVSOR-II at the Institute for Molecular Science, Okazaki, Japan. Data were recorded at room temperature in total electron yield mode, and the X-ray energy dependence of the N Auger electron yield was monitored.

EEL spectra were recorded with a Gatan ENFINA 1000 spectrometer attached to a JEM200CX TEM operated at 200 kV. The detecting system consists of a fiber-coupled YAG scintillator combined with a CCD of 1340 x 100 pixels.

Results and Discussion

The photocatalytic activity reached its maximum at a fluence of 3 x 10²¹ m⁻² and then decreased with the fluence. The sample implanted at a fluence of 5 x 10²¹ m⁻² followed by heat-treatment at 573 K was almost photocatalytically- inactive under visible-light irradiation.

Figure 1 (left) shows N K-edge XANES spectra of the N⁺-implanted TiO₂ samples and a TiN powder for reference. Common XANES features in (a) and (b) suggest that N in the sample implanted by 3 x 10²¹ m⁻² (highest active photocatalyst) is in a chemical environment similar to that in TiN. More thorough observation suggested that double-peak around 400

eV in (b) shifted to the lower energy side compared with that of TiN, which was well reproduced by the theoretical prediction using FEFF code when N occupies one of the O sites of TiO₂. On the other hand, the XANES spectrum of the sample implanted with the N⁺ fluence of 5 x 10²¹ m⁻² followed by heat-treatment (almost inactive to visible-light) shows a distinct single peak around 401 eV (Fig. 1c). This peak could be empirically attributed to formation of molecular species such as N–O bonds near the surface.

Figure 1 (right) shows extracted depth-resolved profiles of the N K-edge ELNES of the samples implanted with the N⁺ fluence of 3 x 10²¹ m⁻². The double-peak structure around 398–401 eV was again observed near the surface region, and the distinct single peak around 401 eV gradually grows with increasing the depth, which reflects the different chemical states of nitrogen, presumably depending on the local N concentration. The double-peak structure near the surface region is in good agreement with the XANES spectrum of the same sample, indicating that N atoms replacing the O sites in TiO₂ dominate up to about 25 nm from the surface. On the other hand the single peak around 401 eV for the deeper regions was observed both in XANES (Fig. 1, c) and ELNES over the entire implanted region of the catalytically inactive sample (the sample implanted at the fluence of 5 x 10²¹ m⁻², followed by heat-treated at 573 K). Considering that the photocatalytic reactions predominate near the surface, the visible-light responsive property should be closely related to the double-peak structure in the XANES/ELNES. Thus, we confirmed that substitutional N at O sites is essential for visible-light responsive photocatalytic activity.

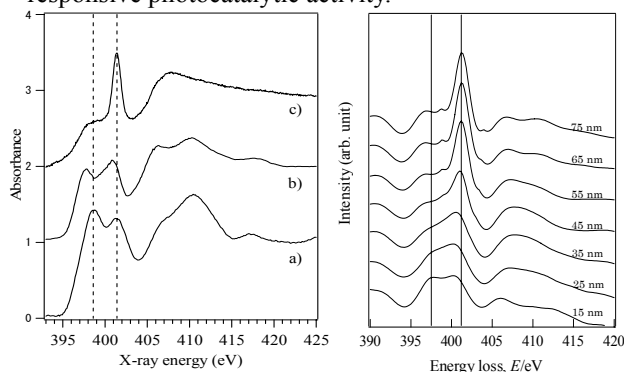


Fig. 1. (left) N K-edge XANES spectra of a TiN(a), N⁺-implanted at 3 x 10²¹ m⁻²(b) and 5 x 10²¹ m⁻² followed by heating at 573 K for 2 h(c), (right) Depth-resolved N K-edge ELNES of photocatalytic active sample, N⁺-implanted with fluence of 3 x 10²¹ m⁻². The numbers inset indicate the depths from the surface.

Photoemission Studies on a Neutral Radical Molecular Crystal of a Tetrathiafulvalene-Based Nitronyl Nitroxide

Y. Nakayama¹, S. Machida², Y. Noguchi^{1,2}, H. Ishii^{1,2},
H. Komatsu³, M. M. Matsushita^{3†} and T. Sugawara³

¹Center for Frontier Science, Chiba University, Chiba 263-8522, Japan

²Graduate School of Advanced Integration Science, Chiba University, Chiba 263-8522, Japan

³Graduate School of Arts and Sciences, The University of Tokyo, Tokyo 153-8902, Japan

Spintronics is a key issue for the next-generation device applications also in the organic electronics field. Requisite materials as a building block of organic spintronics devices are neutral radicals that manifest interactive conductivity and magnetism upon carrier injection. Recently, a neutral radical crystal of 2-[2-(4,5-dibromo-[1,3]dithiol-2-ylidene)-1,3-benzodithiol-5-yl]-4,4,5,5-tetramethylimidazoline-3-oxide-1-oxyl [BTBN; Fig. 1(a)] was synthesized, and the magnetoresistance and narrow-gap semiconducting behavior were discovered on it [1].

In the present study, we conducted the photoelectron spectroscopy (PES) measurements on the BTBN crystals to elucidate the electronic structure of this novel candidate for organic spintronics application.

Needle-like BTBN crystals were produced by electrocrystallization and aligned onto a conductive carbon tape pasted on a polycrystalline Au substrate [Fig. 1(b)]. The both ends of the needles were then bounded by silver paste to ensure good electrical contact. PES measurements were carried out at BL8B2 in UVSOR. During PES measurements, the crystals were illuminated by a violet (405 nm) laser and were biased at +5 V to cancel sample charging that has prevented one from obtaining reliable PES spectra on organic semiconducting crystals [2, 3]. In order to verify the PES results, photoelectron yield spectroscopy (PYS) [4] was also conducted to determine the ionization energy of the BTBN crystal.

Figure 1(d) shows a PES spectrum of the BTBN crystals. The spectral shape looks consistent to the quantum chemical calculation results [Fig. 1(c)], which suggests successful relief of sample charging. The lowest binding energy (BE) component can be assigned to the highest occupied and singly occupied molecular orbitals (HOMO and SOMO). As shown in Fig. 2(a), the carbon tape did not contribute on the PES spectra near the Fermi level. The edge of the lowest BE component is estimated to be 0.5 eV beneath the Fermi level from a line fitting of the peak onset. It corresponds to the ionization energy of 4.85 eV, which is in good accordance to the PYS result. However, by a close look around the Fermi level, one can find a slight tailing further above the HOMO edge [Fig. 2(b)]. This feature also appeared on the PYS spectra. The onset of the tail reached BE ~ 0.1 eV, and it may be an origin of reported sufficient hole

injection even at low temperature [1].

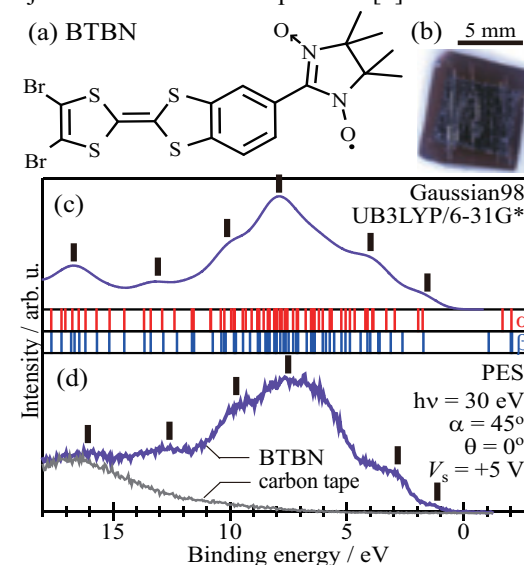


Fig. 1. (a) The chemical structure of BTBN. (b) A photograph of the sample. (c) The “density of states (DOS)” curve obtained by convoluting the molecular orbital energies (vertical bars) with a Gaussian function (FWHM of 1.5 eV). (d) PES spectra of the BTBN crystals and the carbon tape.

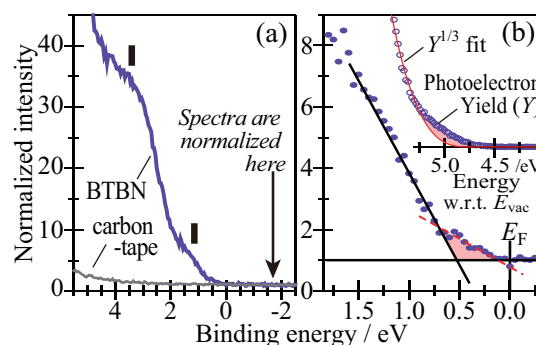


Fig. 2. (a) Magnified PES spectra. (b) PES and PYS spectra of the BTBN crystals.

† Present address: Dept. of Chemistry and Research Center for Materials Science, Nagoya University.

[1] H. Komatsu, *et al.*, *J. Am. Chem. Soc.* in press.

[2] Y. Nakayama, *et al.*, *UVSOR Activity Report 2008 (2009) 70.*

[3] S. Machida, *et al.*, *Phys. Rev. Lett.* in press.

[4] Y. Nakayama, *et al.*, *Appl. Phys. Lett.* 92 (2008) 153306.

Hole Injection Barriers at Organic Hetero-Interfaces in Organic Light-Emitting Diodes

Y. Miyazaki¹, S. Machida¹, Y. Nakayama², Y. Noguchi^{1,2} and H. Ishii^{1,2}

¹Graduate School of Advanced Integration Science, Chiba University, Chiba 263-8522, Japan

²Center for Frontier Science, Chiba University, Chiba 263-8522, Japan

Organic light-emitting diodes (OLEDs) usually have two or more organic layers sandwiched by metal electrodes. At organic hetero-interfaces, carrier accumulation properties play an important role in the device performance, such as the confinement of charge recombination region, providing balanced carriers, and device degradation processes [1-3]. To reveal carrier accumulation mechanisms, we have been investigated this process at various interfaces by using displacement current measurement(DCM) [4, 5].

Carrier injection barriers are a key factor for the carrier accumulation mechanisms. Therefore, it is essential to investigate energy level alignments at interfaces and to know carrier injection barriers. In this study, we investigated energy level alignments by ultraviolet photoelectron spectroscopy (UPS) at 1,3,5-tri(phenyl-2-benzimidazole)-benzene (TPBi), 1,3-Bis[2-(4-tert-butylphenyl)-1,3,4-oxadiazole-5-yl]benzene(OXD-7) and *p*-bis (triphenylsilyl) benzene (UGH2) on 4,4'-bis[*N*-(1-naphthyl)-*N*-phenylamino]-biphenyl(α -NPD) interfaces. Figure 1 shows chemical structures of these materials.

UPS measurement was performed at BL8B2 in UVSOR. Au covered SiO₂ wafers were used as substrates. At first, an α -NPD thin film(10nm) was formed by vacuum deposition on the substrate. Then TPBi, OXD-7 or UGH2 layer was deposited gradually onto the α -NPD film.

Figure 2 shows UPS spectra of TPBi on a α -NPD film. When 6 nm-TPBi was deposited, HOMO peak derived from α -NPD was completely disappeared. Further increase of the TPBi thickness did not change the spectral shape. From the offset of the HOMO edges between 20 nm TPBi and bare α -NPD film, the hole injection barrier is estimated as 1.3 eV. The hole injection barriers at α -NPD/OXD-7 and α -NPD/UGH2 interfaces were estimated as 1.3 eV and 2.0 eV, respectively, in the same manner as the α -NPD/TPBi system. Together with the DCM results, we are now trying to figure out how the observed injection barriers affect electrical behaviors in the actual devices.

[1] J. C. Scott *et al.*, J. Appl. Phys. **89** (2001) 4575.

[2] H. Aziz *et al.*, Science. **283** (1999) 1900.

[3] D. Y. Kondakov *et al.*, J. Appl. Phys. **93** (2003) 1108.

[4] S. Egusa *et al.*, J. Jpn. Appl. Phys. **33** (1994) 2741.

[5] Y. Noguchi *et al.*, Appl. Phys. Lett. **92** (2008) 203306.

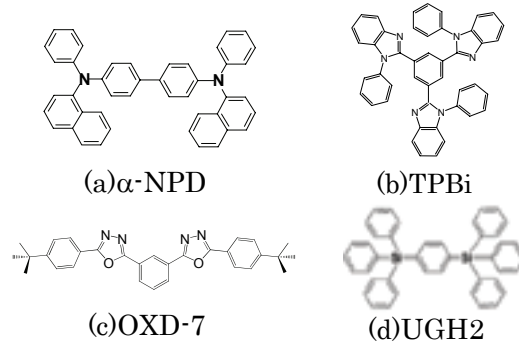


Fig. 1. Molecular structures of materials used in this study.

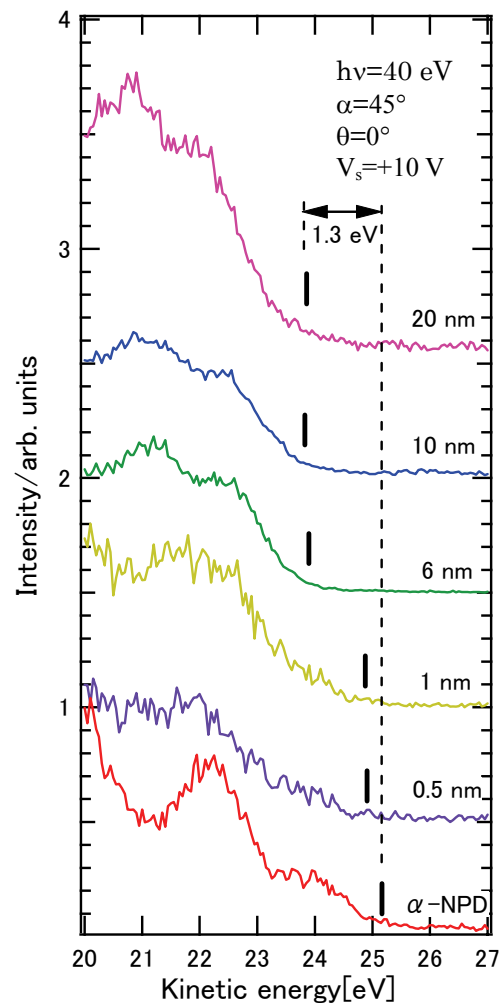


Fig. 2. UPS spectra of TPBi on α -NPD.